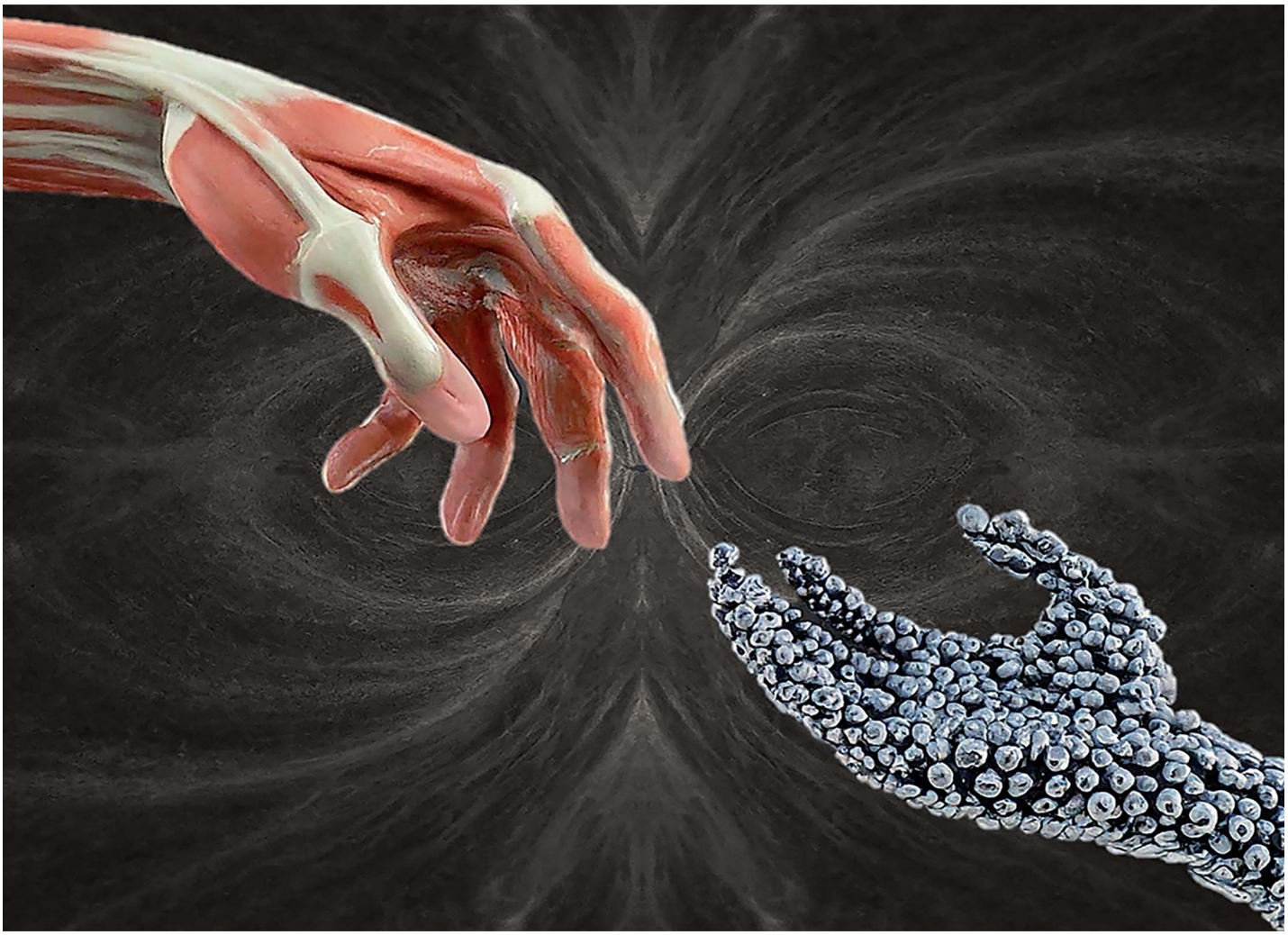

Showcasing research from Assoc. Prof. Monica Focsan's research group, Faculty of Physics, Babes Bolyai University, Cluj Napoca, Romania.

Advancing MRI with magnetic nanoparticles: a comprehensive review of translational research and clinical trials

Enter the transformative realm of contemporary medicine, where Magnetic Resonance Imaging (MRI) stands as a cornerstone, intertwining technology with healing. R. Lapusan and R. Borlan's exploration delves into the integration of Superparamagnetic Iron Oxide Nanoparticles (SPIONs) within MRI, spotlighting their adaptability and safety. From neurological disorders to tumour characterization, SPIONs offer unprecedented precision and potential. Yet, challenges persist, from biocompatibility to iron overload risks. This comprehensive review navigates SPIONs' evolution, from foundational research to cutting-edge applications, offering insights into their journey as MRI contrast agents.

As featured in:

See Monica Focsan *et al.*, *Nanoscale Adv.*, 2024, **6**, 2234.

ROYAL SOCIETY OF CHEMISTRY

rsc.li/nanoscale-advances

Registered charity number: 207890

Nanoscale Advances

ROYAL SOCIETY OF CHEMISTRY

REVIEW

View Article Online
View Journal | View Issue

Open Access Article. Published on 02 4 2024. Downloaded on 2024-08-05 11:52:04.
This article is licensed under a Creative Commons Attribution 3.0 Unported Licence.

Check for updates

Cite this: *Nanoscale Adv.*, 2024, **6**, 2234

Advancing MRI with magnetic nanoparticles: a comprehensive review of translational research and clinical trials

Radu Lapusan,[ab] Raluca Borlan [b] and Monica Focsan *[ab]

The nexus of advanced technology and medical therapeutics has ushered in a transformative epoch in contemporary medicine. Within this arena, Magnetic Resonance Imaging (MRI) emerges as a paramount tool, intertwining the advancements of technology with the art of healing. MRI's pivotal role is evident in its broad applicability, spanning from neurological diseases, soft-tissue and tumour characterization, to many more applications. Though already foundational, aspirations remain to further enhance MRI's capabilities. A significant avenue under exploration is the incorporation of innovative nanotechnological contrast agents. Forefront among these are Superparamagnetic Iron Oxide Nanoparticles (SPIONs), recognized for their adaptability and safety profile. SPION's intrinsic malleability allows them to be tailored for improved biocompatibility, while their functionality is further broadened when equipped with specific targeting molecules. Yet, the path to optimization is not devoid of challenges, from renal clearance concerns to potential side effects stemming from iron overload. This review endeavors to map the intricate journey of SPIONs as MRI contrast agents, offering a chronological perspective of their evolution and deployment. We provide an in-depth current outline of the most representative and impactful pre-clinical and clinical studies centered on the integration of SPIONs in MRI, tracing their trajectory from foundational research to contemporary applications.

Received 29th November 2023
Accepted 1st April 2024

DOI: 10.1039/d3na01064c

rsc.li/nanoscale-advances

[a]*Biomolecular Physics Department, Faculty of Physics, Babes-Bolyai University, Cluj-Napoca, Romania*
[b]*Nanobiophotonics and Laser Microspectroscopy Centre, Interdisciplinary Research Institute on Bio-Nano-Sciences, Babes-Bolyai University, Cluj-Napoca, Romania.*

E-mail: radu.lapusan@ubbcluj.ro; raluca.borlan@ubbcluj.ro; monica.iosin@ubbcluj.ro

Radu Lapusan

Radu Lapusan is a doctoral student at the Faculty of Physics, Babes-Bolyai University, Cluj-Napoca, Romania, with an ongoing research interest focused on using magnetic nanoparticles as contrast agents, mainly for magnetic resonance imaging. He embarked on this journey three years ago, to advance his knowledge and expertise, since this is intricately linked to his primary professional domain, where he serves as a Radiologist, holding the specialist position since 2018 and currently working at the Rehabilitation Hospital in Cluj-Napoca, Romania.

Raluca Borlan

Raluca Borlan, a postdoctoral researcher at the Nanobiophotonics and Laser Microspectroscopy Centre of the Interdisciplinary Research Institute in Bio-Nano-Sciences, Babes-Bolyai University, Cluj-Napoca, Romania, completed her doctoral studies in 2021, proving her dedication and academic excellence in the field. Her focus lies in developing and characterizing nanoparticles for multimodal therapeutic and contrast agent applications. Additionally, she investigates photo-theranostic agent's effects in solution, in vitro, and in vivo, with a focus on cancer therapy and sensing applications. With a solid background in optical spectroscopy and microscopy, Raluca is poised to make significant contributions to nanomedicine.

© 2024 The Author(s). Published by the Royal Society of Chemistry

Open Access Article. Published on 02 4 2024. Downloaded on 2024-08-05 11:52:04.
This article is licensed under a Creative Commons Attribution 3.0 Unported Licence.

1. Introduction

In contemporary medicine, we find ourselves at the intersection of advanced technology and the art of healing. The profound progress in high-tech instrumentation has elevated medical imaging to an indispensable cornerstone of disease diagnosis and treatment. In the realm of medical diagnostics, we harness a plethora of multimodal imaging techniques that delve deep into the human body, providing a comprehensive view of both normal and aberrant anatomy and physiology. Over recent years, the field of medical imaging has undergone remarkable transformation, with each modality offering a unique set of advantages and limitations. Our toolkit now includes a diverse array of techniques, ranging from X-ray and Computed Tomography (CT) scans to Positron Emission Tomography (PET), Single-Photon Emission Computed Tomography (SPECT), digital mammography, diagnostic sonography and MRI.[1]

In the sphere of advanced medical imaging techniques, we find versatile tools serving a broad spectrum of diagnostic purposes, ranging from the detection and evaluation of myocardial diseases, diverse cancer types, neurological disorders, abdominal conditions, among other critical medical conditions. Each imaging modality is finely tuned for a specific application, delivering a precise function in the diagnostic process.[2]

MRI distinguishes itself through its utilization of nonionizing radiation, rendering it the preferred choice in many clinical scenarios over CT. As a noninvasive imaging technique, MRI plays a pivotal role in visualizing the human body's anatomy and physiology, applicable to both health and disease contexts. Notably, it excels in providing intricate contrast for soft tissues, enabling the differentiation between white and gray matter in the brain, making it especially valuable for diagnosing neurological disorders. Moreover, MRI serves as a vital tool in detecting various medical conditions, including ligament and tendon injuries, muscle degeneration, bone tumors, and vascular obstructions.[1,2]

However, it is imperative to acknowledge that despite these advancements, there is substantial room for further enhancement. While our current array of imaging techniques has revolutionized healthcare, opportunities for improvement persist. The integration of novel contrast agents based on nanotechnology presents significant potential, offering avenues to augment medical practice. The exploration of these state-of-the-art solutions has the capacity to reshape the landscape of medicine, potentially ushering in an era marked by even more precise diagnosis and treatment. The journey ahead involves navigating the interface of technology and healthcare, with the ongoing pursuit of a future in which healthcare is boundless in its capabilities.

Monica Focsan

Monica Focsan, PhD since 2010 and Habilitation since 2019, holds the esteemed position of Associate Professor at the Faculty of Physics and Senior Scientific Researcher Grade I at the Nano-biophotonics and Laser Micro-spectroscopy Center, Interdisciplinary Research Institute in Bio-Nano-Sciences (ICI-BNS), Babes-Bolyai University (BBU), Cluj-Napoca, Romania. Her research focuses on nano(-bio)photonics, specializing in the synthesis, and characterization of different versatile nanoparticles with particular morphologies for molecular (bio)sensing, (bio) imaging and therapeutic applications. With over 100 publications, numerous patents, and prestigious awards, including the L'Oreal – UNESCO Fellowship "Women in Science," she is a leading figure in interdisciplinary research at BBU.

2. MRI: principles, functionality and paths to advancement

This painless and noninvasive method is distinguished by its exceptional spatial resolution and the use of nonionizing radiation, solidifying its status as a cornerstone in the analysis of soft tissues. MRI's wide-reaching impact extends as a widely utilized biomedical method for obtaining images of the body's water-containing soft tissues. This is achieved by applying an external magnetic field to the sample, forcing the water proton's magnetic poles to line up with the field. Then, a brief radio-frequency (RF) pulse is applied at a frequency that is the same as the hydrogen atom's resonance frequency. When the RF pulse is finished, the protons release an RF signal which the MRI equipment detects and uses to create images. The short delay between RF pulses allows protons to relax and realign with the external magnetic field before changing the orientation again with the next RF pulse. The tissue's relaxation time is the duration needed by the protons (primarily those of water) to return to the initial configuration.

There are typically two main types of relaxation times: longitudinal relaxation time, or T_1, and transverse relaxation time, or T_2.[3] In MRI sequences, tissue and fluid shades are described using intensity terms, which correlate with their relaxation times. High signal intensity, appearing as white on the grayscale used for image formation, often corresponds to shorter relaxation times, such as T_1 relaxation. Conversely, low signal intensity, appearing as black, typically relates to longer relaxation times, such as T_2 relaxation. Intermediate signal intensity, depicted as grey, usually indicates a balance between T_1 and T_2 relaxation times. These intensity levels are represented on a grayscale, with brighter areas indicating higher signal intensity and darker areas indicating lower signal intensity in the resulting MRI images.

T_1, also known as spin–lattice relaxation, describes the process by which the net magnetization vector returns to its equilibrium value along the direction of the external magnetic field. It's often called longitudinal relaxation because it occurs

Open Access Article. Published on 02 4 2024. Downloaded on 2024-08-05 11:52:04.
This article is licensed under a Creative Commons Attribution 3.0 Unported Licence.

along the direction of the external magnetic field. Tissues with a short T_1 relaxation time will appear bright on T_1-weighted images, images used for visualizing anatomy and assessing lesions, such as in the brain where gray matter appears bright and white matter appears dark. On the other hand, T_2, or spin–spin relaxation, refers to the process by which the net magnetization vector in the plane perpendicular to the external magnetic field returns to equilibrium. It's called transverse relaxation because it occurs in a direction transverse to the external magnetic field and tissues with a long T_2 relaxation time will appear bright on T_2-weighted images. These images are valuable for detecting pathology, such as inflammation or edema, where affected areas often appear bright. Both T_1 and T_2 relaxation times are fundamental concepts in MRI and have important implications for image contrast. They are specific to each type of bodily tissue and largely depend on their water content, allowing for differentiation between various tissues.[4]

To further enhance MRI's imaging abilities, specialized contrast agents have been developed to alter these relaxation times. Gadolinium-based contrast agents, the currently preferred T_1 contrast agents for MRI, act by shortening the T_1 relaxation time of the water protons neighboring gadolinium (Gd) complexes, which leads to a brighter signal on the T_1-weighted imaging sequence, therefore exhibiting positive contrast capabilities. Unfortunately, Gd in its pure form is very toxic to humans; it can lead to nephrogenic systemic fibrosis in patients with poor renal function.[3] Gd has been shown to accumulate dose-dependently in the brain independent of renal function, as well as in other tissues (bone, liver, spleen, skin and kidney), but a link between this Gd deposition disease and clinical manifestations have yet to be demonstrated.[5] Thus, it is becoming increasingly apparent that the current contrast agents, including gadolinium-based ones, have their limitations, especially concerning toxicity and their distribution within the body. This has prompted a quest for alternative contrast agents that could address these issues. While inorganic nanoparticles (NPs) like Gd oxide, Gd fluoride, and Gd phosphate are increasingly being explored as alternatives due to their small size and magnetic properties, they also come with their own set of limitations.

Consequently, researchers have expanded their focus to explore a broader spectrum of inorganic NPs, each with its unique characteristics. This exploration aims to identify alternative agents that can effectively overcome the limitations associated with traditional contrast agents. The field of inorganic NPs-based MRI has witnessed significant advancements, including the utilization of targeted Gd_2O_3 NPs, the creation of dual-function T_1–T_2 MRI probes, the development of hybrid MRI/fluorescent probes, and the introduction of theranostic agents specifically designed for tumor imaging. These innovations have showcased the remarkable potential of inorganic NPs in enhancing the precision and efficacy of MRI diagnostics. Notably, a study found PEGylated-Gd_2O_3 NPs to offer longer blood half-life, enhanced MRI contrast, and reduced toxicity compared to the commercial Magnevist.[6] Recent advancements include the synthesis and characterization of dual contrast agents based on polydopamine NPs (PDA-NPs) targeted with hyaluronic acid (HA) and chelated with Gd^{3+}. The PDA/HA/Gd^{3+} NPs demonstrated low cytotoxicity, enhanced stability in water, and targeted binding to $CD44^+$ cancer cells. In imaging tests, they showed comparable or superior contrast capabilities to commercial contrast agents such as Dotarem and Barium sulfate, with higher relaxivity in MRI.[7] These demonstrate the tangible benefits that nanotechnology can bring to the field of MRI contrast agents.

In conclusion, while current contrast agents, including various Gd-based NPs, have played a vital role in advancing MRI technology, the exploration of nanotechnology and a wider array of inorganic NPs offers a promising avenue for improvement. These advancements hold the potential to overcome the limitations associated with traditional agents, potentially revolutionizing the field of medical imaging and offering new possibilities for enhanced diagnostics and therapies.

3. Magnetic nanoparticles in MRI: current insights and the pursuit of enhancement

With these challenges and innovations in mind, the following section delves into the promising frontier of magnetic NPs as contrast agents for MRI, exploring their potential to overcome existing limitations and transform the field of medical imaging. Precisely, iron oxide particles have emerged in the last 30 years as a safe and highly customizable alternative to Gd-based contrast agents. They have an iron oxide core, with variations such as magnetite (Fe_3O_4), maghemite, and hematite (Fe_2O_3) existing in different phases. Notably, hematite exhibits weak ferromagnetism. This distinction is crucial for understanding the magnetic properties of NPs. Furthermore, these NPs playing a significant role in MRI contrast enhancement, having the capability to alter both T_1 and T_2 relaxation times.[8] These superparamagnetic capabilities of SPIONs are strongly influenced by the size, shape and coating of the particles (Fig. 1). Optimally we are looking for a narrow size distribution with homogenous physical and chemical properties, while alterations in shape can change the exposed crystal facets and the corresponding atomic arrangements within those facets, leading to significant effects on various properties, such as binding affinity, rate of tumor deposition or therapeutic efficacy.[9,10] Based on the size range within which they reside, iron oxide particles can be divided into three categories: micro-sized iron oxide particles, approx. 1 μm (MPIOs); standard superparamagnetic iron oxide particles, 5–150 nm (SPIOs); and ultrasmall superparamagnetic iron oxide particles, 5–50 nm (USPIOs).[11]

Moreover, SPIONs can create local field inhomogeneity in the tissue of choice, effectively reducing signal intensity in T_2-weighted sequences (negative contrast) and increasing signal intensity in T_1-weighted sequences (positive contrast). As experiments show, the T_2 relaxation increases with an increasing core diameter, in contrast to the T_1 shortening effect, which increases with a decreasing core diameter. Consequently, SPIONs with small core diameters function as signal amplifiers

 © 2024 The Author(s). Published by the Royal Society of Chemistry

Open Access Article. Published on 02 4 2024. Downloaded on 2024-08-05 11:52:04.
This article is licensed under a Creative Commons Attribution 3.0 Unported Licence.

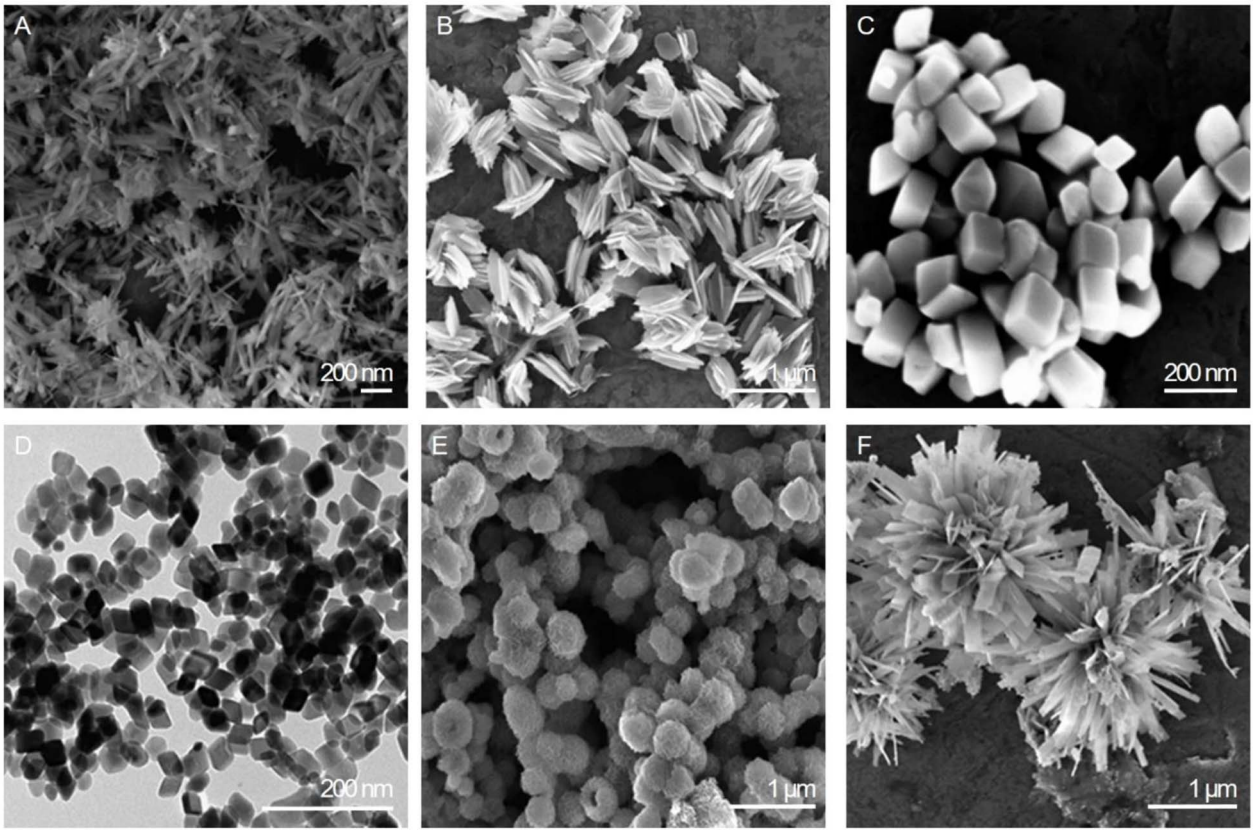

Fig. 1 Electron microscopy images of six distinct shapes of iron oxides: (A) nanorods, (B) nanohusks, (C) distorted cubes, (D) nanocubes, (E) porous spheres, and (F) self-oriented flowers. Modified with permission from Sayed, F., Polshettiwar, V. (2014)[9] Creative Commons – Attribution 4.0 International – CC BY 4.0 (https://creativecommons.org/licenses/by/4.0/).

in T_1-weighted sequences, while SPIONs with large core diameters are suitable for applications using the signal reduction in T_2-weighted sequences. All commercially available SPIONs contrast agents are working as T_2 contrast agents and reside in the range of 16–150 nm (hydrodynamic diameter).

Nonetheless, T_1 and T_2 are not the only MR sequences used in imaging SPIONs. Gradient echo sequences (GRE, FFE) are more sensitive to magnetic susceptibilities than spin echo sequences (SE), and this sensitivity is increased by decreasing the flip angle, extending the echo or repetition time and increasing spatial resolution.[12] Other developments use susceptibility-weighted imaging (SWI) to improve tissue contrast with a positive contrast agent[13,14] or even without a contrast agent[15,16] using magnitude and phase information from the complex data of spatially highly resolved 3D gradient echo sequences and suitable post-processing algorithms that create susceptibility/phase gradient maps.[17]

3.1 The evolution of magnetic nanoparticles in clinical MRI

The first commercially available iron oxide NP solution was approved in 1996[18] by the Food and Drug Administration (FDA), had a hydrodynamic size of 40–150 nm (Standard SPIOs), used a dextran coating and were designed for liver imaging (ferumoxide (Endorem^R/Ferridex^R), ferucarbotran (Resovist^R)). One unforeseen side effect for Ferridex^R was a severe backache after bolus injection. Due to several side effects and lack of demand, Ferridex^R has been withdrawn from the market since 2011 and Resovist^R is currently available only in limited countries, like Japan. Other agents followed in 2011, namely ferumoxtran (Combidex^R) used initially for prostate cancer lymph node metastasis imaging, and ferumoxytol (Feraheme^R), designed for addressing iron deficiency anemia in patients with chronic kidney disease. These agents had a smaller core and hydrodynamic size, paving the way for the new USPIOs in the range of 20–40 nm. However, ferumoxytol proved some side effects and the FDA gave a black box warning regarding serious hypersensitivity/anaphylaxis reactions. But despite these limitations, ferumoxytol is among few SPIONs formulations being used today, both for the proposed application and also off-label as an MRI angiography agent in patients that cannot use Gd.[8] Another notable mention are formulations used as oral gastrointestinal contrast agents, namely *ferumoxsil* (Gastro-MARK^R(EU), Lumirem^R(USA)) and *ferristene* (Abdoscan^R). They belong to standard SPION type, are coated with insoluble materials (siloxane and polystyrene, respectively) and are marked as safe and effective. Ferumoxsil is today the only iron oxide NPs approved by the FDA for imaging purposes, namely gastrointestinal and bowel imaging.

Open Access Article. Published on 02 4 2024. Downloaded on 2024-08-05 11:52:04.
This article is licensed under a Creative Commons Attribution 3.0 Unported Licence.

3.2 Prospects for improved magnetic nanoparticles

While magnetic NPs have shown promise in medical imaging during the last years, challenges have arisen. Some formulations faced side effects, but advancements are continually being pursued to develop even more effective magnetic NPs for enhanced medical imaging applications.

Standard SPIOs (over 50 nm in diameter) have been faulted for (1) inadequate renal clearance after intravenous (i. v.) administration due to their large hydrodynamic size, which leads to accumulation in the body and generate persistent negative contrast spanning weeks or months, preventing further imaging investigations and hindering clinical management; and (2) the absorption in the body's iron pool can lead to clinical side effects from iron overload. Consequently, classes of positive contrast agents with very small hydrodynamic diameter are in clinical trials as we speak.[19] These endeavors include exploring surface functionalization with advanced materials to enhance NP performance. Adding hydrophilic molecules on their surface balances the water molecules around SPIONs, further assisting in lowering T_2 relaxation time. The smallest currently synthesizable iron oxide NP has a core diameter of 3–4 nm and a particle size of 5–7 nm with a monomer coating, namely very small SPIONs.[20–23]

For MRI applications, commonly used coatings enumerate poly(ethylene glycol) (PEG), poly(vinylalcohol) (PVA), or natural polysaccharides (dextran and modified chitosan), mostly owing to their lengthy shelf-life. SPIOs with neutral/hydrophilic surface and small size are phagocytized and opsonized slower than SPIOs with ionic/hydrophobic coating. Hence, in the case of standard SPIOs, monocytes and macrophages of the reticuloendothelial system (RES) remove them from the blood stream, granting a short blood half-life (*e.g.*, 8 minutes for ferumoxide). They mostly concentrate in the liver (80–90%), spleen and bone marrow. By comparison, USPIOs and very small SPIOs have a longer blood half-life (*e.g.*, 10–14 h for ferumoxytol) and can be used as blood pool contrast agents.[9,23]

The phagocytosis of SPIONs by RES organs is one of the targeting mechanisms that can be used to detect lesions in the liver, spleen, lymph nodes and bone marrow. Other passive targeting mechanisms encompass the enhanced permeability and retention (EPR) effect, nanoparticle-induced endothelial leakiness, using the tumor acidic microenvironment, or phagocytosis by inflammation-related macrophage. The EPR effect allows i. v. administered NPs to extravasate and concentrate in tumor tissue, with the percentage varying by tumor type. This effect is utilized by several clinically-approved drug nanoformulations, including Doxil™ and Abraxane™.[24]

In the absence of any EPR effect, SPIONs can bear a process called nanoparticle-induced endothelial leakiness, which rearranges the cytoskeleton by inducing gaps of over 10 μm between endothelial cells and occurs faster than phagocytosis.[25] Moreover, using a surface charge switch triggered by the tumor's acidic microenvironment, SPIONs conjugated with pH-sensitive ligands can be activated to generate contrast and can even prompt the formation of singlet oxygen species. Last but not least, inflammation-related macrophages that can be associated with cancerous tissue but also with benign conditions like atherosclerotic plaques can also be targeted by the same mechanisms that target RES organs.[26]

Thus, bearing these considerations in mind, the strategic selection of characteristics encompassing size, shape, and surface material for functionalization holds the potential to empower the next generation of magnetic NPs. These new and enhanced magnetic NPs can broaden their capabilities, extending to specialized applications such as lymph node imaging, inflammation assessment, infection detection, vascular evaluation, cell tracking and precise tumor identification and localization. This underscores the exciting prospects for advanced MRI contrast agents with enhanced performance.

4. Next-generation magnetic nanoparticles in MRI: translating research to clinical trials

In contemporary clinical practice, the utility of SPIONs has extended far beyond their initial applications. These versatile NPs have found widespread use owing to their unique properties that enable both T_1 and T_2 relaxation shortening effects.

The most prominent role of SPIONs in clinical settings lies in harnessing their T_1 and T_2 relaxation properties. This dual functionality has opened the door to a spectrum of applications, with SPIONs demonstrating their efficacy in both T_2/T_2^* and T_1-weighted imaging; T_2/T_2^* imaging capitalizes on SPION accumulation within tissues, delivering enhanced contrast and enabling precise visualization of various anatomical structures and pathological conditions. In parallel, the T_1 effect of SPIONs comes into play during their circulation within the bloodstream, further expanding their diagnostic potential.

This section delves into the extensive body of research and clinical trials that exemplify the transformative impact of SPIONs in MRI. Through a series of subsections, we explore the diverse studies and investigations that have harnessed SPIONs to advance medical imaging and patient care. From their utilization in characterizing liver lesions to monitoring lymph node metastases, SPIONs have ushered in a new era of diagnostic precision. As we navigate through these studies and trials, it becomes evident that SPIONs have become indispensable tools in the hands of clinicians and researchers. Their versatile applications and evolving formulations are paving the way for the next generation of magnetic NPs in MRI.

4.1 Inflammation imaging

Inflammation processes can be visualised by the high uptake of SPIONs in the macrophages. Assessing the inflammatory status of carotid plaques is an essential step in evaluating plaque instability and vulnerability to rupture and subsequent thromboembolism. Trivedi *et al.*[27] proved in 2006 that USPIO-enhanced MRI is competent in detecting plaque inflammation *in vivo*, identifying high-risk patients. The ATHEROMA study[28] conducted in 2009 linked an aggressive lipid-lowering therapy with an important reduction in USPIO-defined inflammation, offering value to the previous study. Further proof was

 © 2024 The Author(s). Published by the Royal Society of Chemistry

Open Access Article. Published on 02 4 2024. Downloaded on 2024-08-05 11:52:04.
This article is licensed under a Creative Commons Attribution 3.0 Unported Licence.

presented by Morishige *et al.*[29] one year later when the detectable signal loss in USPIO-enhanced MRI was proven to be proportionate to the degree of inflammation present, allowing the quantification of atherosclerotic plaques burden. Recent research has taken this confirmed technique to the next level. In 2019, Zheng *et al.*[30] detected femoral artery plaque inflammation with ferumoxytol-enhanced MRI and revealed a good correlation with dynamic gadolinium-enhanced MRI. In 2022, Chan *et al.*[31] developed a smart MRI probe using dual-targeted microparticles of iron oxide against P-selectin and VCAM-1 which allows very accurate risk stratification and is ready to be translated into clinical setting. Bonnet *et al.*[32] made one of the first steps towards a theranostic approach to this area in 2021 when nano-emulsions of SPIONs functionalized to target galactin 3, an atherosclerotic biomarker, were loaded with alpha-tocopherol in order to reduce plaque oxidation. Recently, Segers *et al.*[33] found that ferumoxide and ferumoxtran induce apoptosis in lipid-laden macrophages in both human and murine atherosclerosis, effect that can be avoided by using concomitant antioxidant treatment. However, this effect was not observed with ferumoxytol. These findings have significant implications for patients with advanced atherosclerosis, as they might influence disease progression, so not all results are positive.

The gold standard of imaging neuro inflammation *in vivo* is PET-CT with radiotracers in clinical setting and two-photon microscopy with fluorescent dyes in preclinical setting. While the latter has drawbacks that will not allow it to be translated into clinical practice (skull absorption of light, low penetration), the former has both its general technique disadvantages and limitations regarding acute inflammation in stroke, for example.[34] In recent decades, USPIO-enhanced MRI have been used to track phagocytic cells in the central nervous system for various pathologies. The mechanism of enhancement different for SPIONs and for Gd. While the latter presents nonspecific inflammation data that only evaluates the integrity of the blood–brain barrier (BBB), the former is taken up directly by macrophages and can additionally identify their content and infiltration degree.[35] Several studies in multiple sclerosis patients have proven the ability of ferumoxtran-10, when compared with Gd-enhanced MRI, to find new active lesions not detected by Gd and pinpoint lesions with aggressive behaviour, that are enhanced by both contrast agents.[36] In the future, this dual technique should find it's way to clinical practice, although at this time the clinical studies are still in phase 1.

In stroke patients, macrophage response to brain ischemia can be noninvasively monitored, helping in targeting anti-inflammatory therapy to select cases.[37] Furthermore, the works of Walter *et al.* in 2015[38] and others before him[39,40] have suggested that USPIOs can be a noninvasive method of tracking prognosis of ischemic stroke by setting apart inflamed brain regions without phagocytes that tend to remain viable in the long run. Fig. 2 contrasts MRI images before and after administering USPIO in a patient with a right middle cerebral artery infarction, showing occlusion and thrombus hypointensity before USPIO, followed by USPIO-related enhancement and blood–brain barrier disruption afterward.[39] Ferumoxytol is also extensively studied in this sector. Hasan *et al.* tracked macrophage response in a brain aneurysm, selecting unstable lesions[41] and showing reduced wall inflammation after aspirin treatment.[42] Wall inflammation can also be observed for brain arteriovenous malformations[43] and abdominal aortic aneurisms. In the latter case, it can provide morphologic assessment of thrombus organisation and can mark phagocytic leukocytes, electing high-risk aneurysms.[44] Khan *et al.*[45] showed that migraines without aura are not associated with macrophage-mediated inflammation, offering new pathways in understanding migraine pathophysiology.

The kidneys can also benefit from SPION-derived imaging techniques. First of all, it can provide useful morphological analysis by measuring the number and size of all the glomeruli in the entire kidney[46] or asses the structural integrity of the basement membrane.[47] Second of all, because inflammation is the main pathway to kidney fibrosis and end-stage kidney disease, diagnosis and quantification of said inflammation is of utmost importance, especially in the setting of current radiological or serological techniques that provide inconsistent and non-reproducible data. Kidney inflammation is also the main pathway of type I and II diabetes of progressing to kidney failure, owing to the proinflamatory cytokine production following hyperglycemia and hypertension. Current gold standard of assessing renal inflammation is kidney biopsy with histopathological study, which is an invasive technique that only scrutinizes 0.01% of kidney tissue; as a result about only 10% of patients undergo the procedure.[48] Non-targeted SPIONs have been proven to accumulate in kidney macrophages by several studies, including Serkova *et al.* in 2010,[49] and can be used to monitor kidney transplantation and transplant rejection.[50] Targeted SPIONs have been proven to detect kidney inflammation in several pathologies that, if left untreated, eventually progress to end-stage kidney disease. Wu *et al.*[51] developed in 2021 $\alpha_v\beta_3$-targeted superparamagnetic Fe_3O_4 NPs for imaging of integrin $\alpha_v\beta_3$, which is overexpressed in IgA nephropathy (the most common glomerular disease in the world). Serkova *et al.*[49] used C3d conjugated NPs to weigh renal inflammation in a mouse model of lupus nephritis.

Inflammatory diseases of the bowel, namely Crohn disease and ulcerative colitis, can also be evaluated by taking advantage of macrophage uptake of SPIONs. Wu *et al.*[52,53] presented in 2013 both the ability of detecting the presence of a pathologic process and also the quantitative assessment of disease activity, using Feridex *in vivo*.

Inflammation is also prompted by obesity at the level of the adipose tissue, leading to macrophage infiltration that is directly related to obesity-associated comorbidities. Luciani *et al.*[54] showed in 2012 the ability to use USPIO-enhanced MR as an imaging biomarker[55] for patients at risk for metabolic syndrome.

4.1.1 Infection imaging. Inflammation and infection are closely related pathological processes. Following the development of macrophage tracking in inflammation processes, this technique was also adopted for infection detection.

SPION-based contrast agents have shown promising results in animal studies for MRI of infections. For example, studies by

Open Access Article. Published on 02 4 2024. Downloaded on 2024-08-05 11:52:04.
This article is licensed under a Creative Commons Attribution 3.0 Unported Licence.

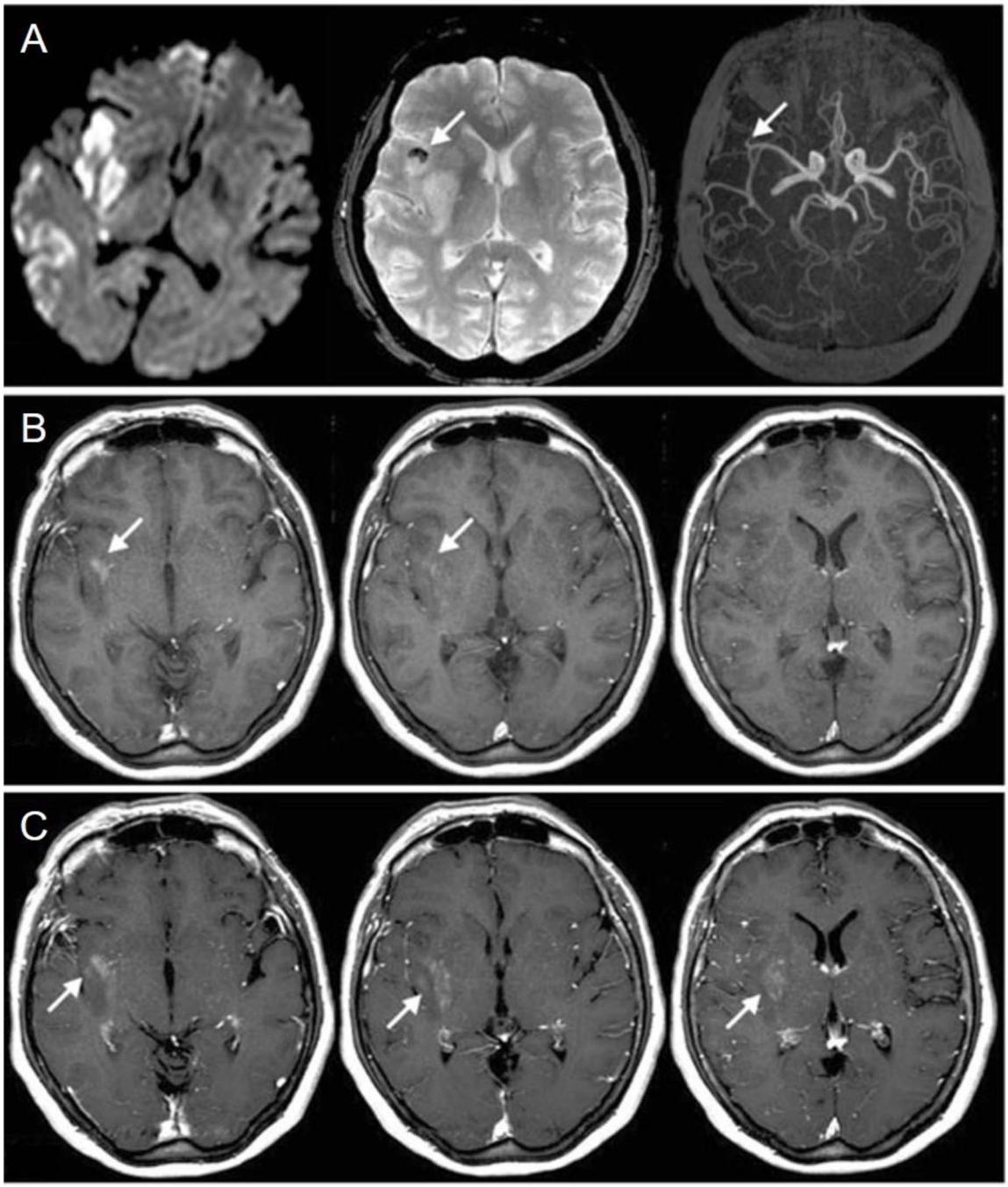

Fig. 2 Comparison between MRI images taken on the second day before the administration of USPIO (pre-USPIO) and on the fourth day after its administration (post-USPIO) in a patient with a right middle cerebral artery infarction. (A) From (left) to (right): pre-USPIO diffusion-weighted imaging (DWI), T_2^*-weighted imaging (T_2WI), and time-of-flight magnetic resonance angiography (TOF MRA) revealing occlusion of an insular branch (indicated by arrows); the thrombus appears hypo intense on T_2WI (arrow). (B) Pre-gadolinium T_1-weighted imaging (T_1 WI) displaying focal enhancement within the infarct region, attributed to USPIO (arrows). (C) Post-gadolinium T_1 WI showing disruption of the BBB extending beyond the USPIO-related enhancement (arrows). Copyright (2008), with permission from John Wiley and Sons.[39]

Lefevre *et al.*[56] have shown a marked MR signal intensity loss in the septic knees of rabbits injected with SPIONs (Fig. 3). MR imaging tracked septic arthritis progression in a rabbit knee during antibiotic therapy, revealing synovitis and synovial thickening on unenhanced T_2^*-weighted images during acute infection, followed by signal intensity loss due to iron-loaded macrophage infiltration after USPIO injection. The degree of T_2-weighted signal intensity loss in SPION-treated subjects was found to correlate with the iron content in the imaged area. Furthermore, Bierry *et al.*[57] showed that Gd alone was unable to distinguish osteomyelitis from sterile inflammation induced by mechanical damage in rabbit vertebral osteomyelitis, but SPIONs were effective for this purpose. This distinction could be

 © 2024 The Author(s). Published by the Royal Society of Chemistry

Open Access Article. Published on 02 4 2024. Downloaded on 2024-08-05 11:52:04.
This article is licensed under a Creative Commons Attribution 3.0 Unported Licence.

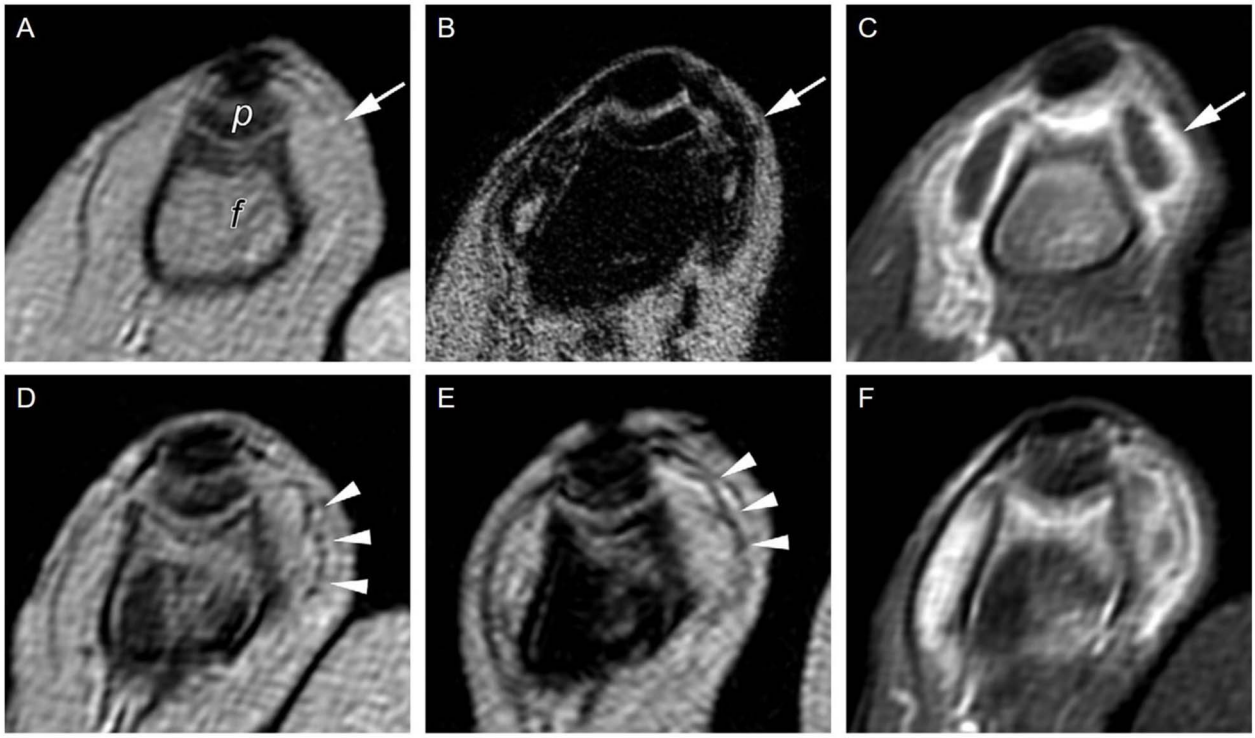

Fig. 3 Sequential axial MR imaging tracking the progress of septic arthritis in a rabbit knee during intravenous antibiotic therapy. In the acute infection phase (A), visible synovitis with synovial thickening (arrow) is depicted on an unenhanced T_2^*-weighted gradient-echo image, with reference to the femur (f) and patella (p). (B) Within 24 hours of USPIO injection, a pronounced signal intensity loss occurs due to iron-loaded macrophage infiltration (arrow) in the synovium, as seen on a T_2^*-weighted image. (C) Synovitis with signal enhancement (arrow) is observed on a gadolinium-enhanced T_1-weighted image. After antibiotic therapy (D), the T_2^*-weighted gradient-echo image reveals only focal areas of signal intensity loss in the synovium (arrowheads), which do not intensify on an image acquired 24 hours after USPIO re-administration (E). (F) Gadolinium uptake remains visible in the synovium on a gadolinium-enhanced T_1-weighted image. Copyright (2011), with permission from Radiological Society of North America.[56]

made because macrophages are relatively sparse in areas of noninfectious degenerative change.[58]

In conclusion, SPION-based contrast agents show potential in MRI for detecting infections by tracking macrophages, which play a key role in both inflammation and infection processes. Additionally, SPION-enhanced MRI demonstrates significant potential in various inflammation-related applications. It aids in visualizing inflammation processes, particularly in carotid plaques, quantifying atherosclerotic plaque burden, and providing insights into plaque stability. This technique also proves valuable in neuro inflammation, enabling non-invasive detection and monitoring of conditions like multiple sclerosis and stroke, including prognosis assessment. Furthermore, SPION-enhanced MRI offers non-invasive alternatives for kidney assessment and shows promise in inflammatory bowel diseases and obesity-related inflammation. Overall, SPION-enhanced MRI expands non-invasive imaging capabilities in various medical domains, enhancing patient care and diagnosis, with ongoing research poised to advance its applications further.

4.2 Vascular imaging

Vascular imaging techniques will be taking advantage of the T_1 shortening effects of SPIONs for the first time in this chapter. Magnetic resonance angiography (MRA) is a non-invasive medical imaging technique that uses MRI technology to visualize blood vessels and the flow of blood within the body. Not surprisingly, using contrast enhancement is a mainstay of vessel imaging, and SPION-based formulations have been comprehensively tested for this purpose in the last two decades. One of the first feasibility studies was published in 1999 when Schmitz *et al.*[59] demonstrated good or sufficient arterial pulmonary, whole-body and lower extremity venous system visualisation in all 12 adult patients, clearly demonstrating a femoral vein thrombosis. Also in 1999, Ahlström *et al.*[60] acquired high-quality MRA of pulmonary vasculature using Clariscan™. One of the first times magnetic NPs gained public attention as blood pool agents was in 2004, in a phase 2 study, when Prince *et al.*[61] used ferumoxytol to reveal more aortic stent-graft endo-leaks 24 h after administration compared with CT angiography (using Gd-based products), especially detecting small and slow leaks. Ferumoxytol's coating prevents redistribution outside the vascular space, enabling delayed MRA image acquisition. This prolonged blood circulation time was further investigated in 2016 by Corwin *et al.*,[62] who compared steady-state MRA (prolonged acquisitions that improve signal-to-noise ratio and consequently spatial resolution) with first-pass MRA, yielding a similar vessel sharpness and equivalent signal-to-noise ratio between the two.

Open Access Article. Published on 02 4 2024. Downloaded on 2024-08-05 11:52:04.
This article is licensed under a Creative Commons Attribution 3.0 Unported Licence.

Several clinical phase I trials have been performed yielding promising results. In 2011, Wagner *et al.*[63] showcased a moderate diagnostic accuracy for detecting significant coronary artery stenosis on coronary MRA using VSOP-C184 (very small superparamagnetic iron oxide particles, 184th variant of a citrate-coated preparation, batch number 050701), a USPIO formulation (Fig. 4). Identification of coronary artery disease is demonstrated through contrast-enhanced coronary MR angiography following the injection of 20 mmol Fe per kg of VSOP-C184, with occlusion confirmed by invasive coronary angiography. Although replacing CT angiography for visualisation of coronary artery disease has several advantages, including no exposure to ionizing radiation, Sakuma *et al.*[64] presented in the same year the main drawbacks, namely long image time, lower spatial resolution, and operator dependency. Nevertheless, an ongoing phase 3 trial[65] is currently testing coronary artery visualisation using ferumoxytol in a cohort with reduced kidney function.

The precise measurement of rCBV was taken a step further by Timms and his colleagues by developing a method called Quantitative Ultra-Short Time-to-Echo Contrast Enhanced (QUTE-CE) MRI which is well suited for measuring quantitative cerebral blood volume (qCBV), creating a 3D MRI rat brain atlas in 2017.[67] Correlating results from awake resting-state and under isoflurane anesthesia showed significant decrease in qCBV in the neural circuitry of memory and primary senses of smell, hearing and vision (suggesting a role in consciousness) and an increase in the neural circuitry of automated functions, like preserving respiration, body temperature or cardiovascular function. Furthermore, Thrippleton *et al.*[68] developed a protocol for evaluating cerebral small vessel disease; owing to the fact that MRI relaxometry allows USPIO uptake quantitative evaluation, they were able to measure cerebral parenchymal uptake and BBB leak.

The use of gadolinium-based contrast agents in individuals with kidney disease is a significant worry due to the potential risk of nephrogenic systemic fibrosis (NSF), a serious systemic condition first identified in 1997 in patients with kidney impairment. To prevent the occurrence of NSF in kidney disease patients, it is imperative to seek a safer alternative contrast medium that can offer comparable enhancement.[69] For instance, individuals with kidney failure usually depend on hemodialysis to cleanse their blood, achieved through an arteriovenous fistula. Sigovan *et al.*[70] revealed significant better performance of ferumoxytol-enhanced MRA in imaging hemodialysis fistulas as compared to non-enhanced time-of-flight MRA, greatly reducing flow artifacts. In line with the same pathology, renal graft functionality is commonly evaluated using non-enhanced ultrasound, which can yield inconclusive results. Thus, contrast-enhanced MRA proves beneficial but needs a novel contrast agent. Zamecnik *et al.*[71] showed excellent image quality and visibility of pelvic arteries using ferumoxtran-10-enhanced 3T MRA. Timms *et al.*[72] optimised their QUTE-CE MRI for the view of kidney vasculature, yielding great detail of renal anatomy or renal cysts and enabling quantitative morphometric analysis of abdominal and renal vessels.

Moving forward, in 2021 Shin *et al.*[73] tested NPs with a polysaccharide supramolecular core and a shell of amorphous-like hydrous ferric oxide for the visualisation of cerebral, coronary and peripheral microvessels in rodents and of lower-extremity

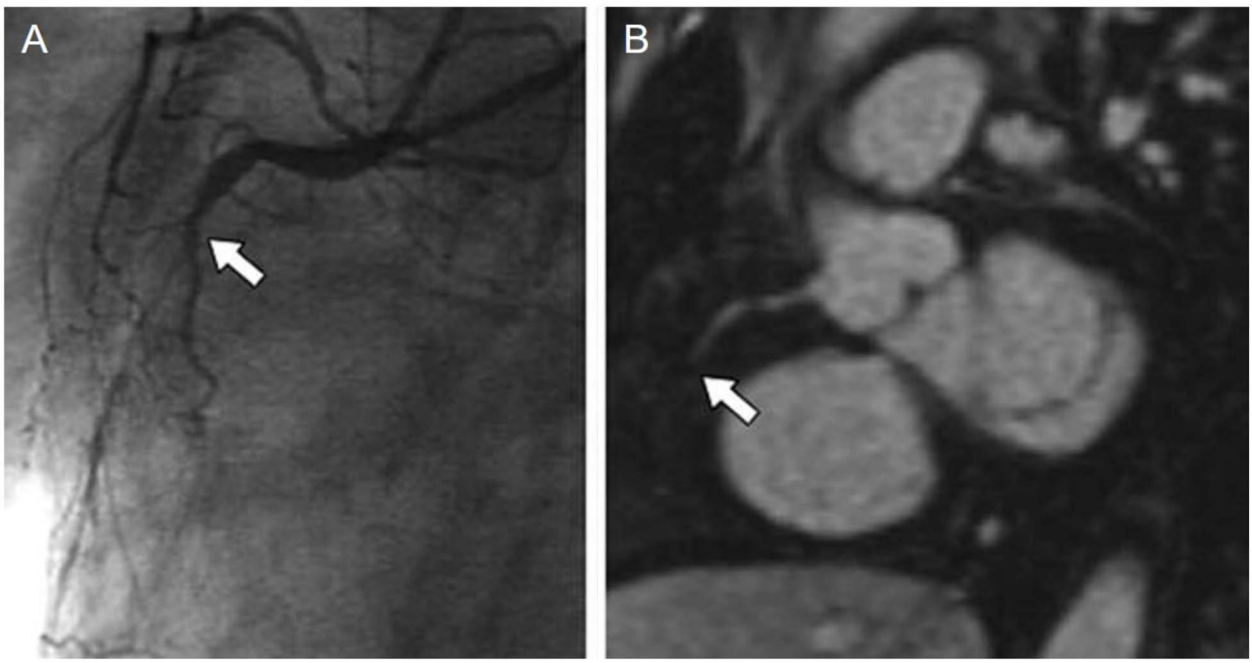

Fig. 4 Identification of coronary artery disease through contrast-enhanced coronary MR angiography following the injection of 20 mmol Fe per kg of VSOP-C184. (A) Invasive coronary angiography confirmed the presence of occlusion in the middle part of the right coronary artery (indicated by the arrow). (B) Notably, contrast-enhanced coronary MR angiography distinctly visualizes this occlusion (indicated by the arrow). Copyright (2011), with permission from John Wiley and Sons.[66]

 © 2024 The Author(s). Published by the Royal Society of Chemistry

Open Access Article. Published on 02 4 2024. Downloaded on 2024-08-05 11:52:04.
This article is licensed under a Creative Commons Attribution 3.0 Unported Licence.

vessels in rabbits, showing better imaging performance than a Gd-based contrast agent, gadoterate meglumine. This is being tested in a phase 1 ongoing clinical trial[74] as we speak.

Buch *et al.* used susceptibility-weighed MRI sequences (T_2^* dominant approach) to image microvasculature in several studies. In 2020[75] they illustrated midbrain microvasculature, acquiring data at different time-points in order to avoid blooming artifacts of large vessels and detecting small vessels in the order of 50–100 μm. Next year, they were able to display vascular abnormalities and the density of small vessels in multiple sclerosis lesions, providing new insights into disease pathophysiology.[76] In 2022,[77] they successfully mapped hippocampal microvasculature, also quantifying tissue fractional vascular density in each of the subfields of the hippocampus; their results suggest that vascular degeneration precede tissue atrophy and are consequently able to measure atrophy and volumetric changes. This data strongly correlated both with ageing and with several neurodegenerative diseases, giving insights into disease etiology. Clinical trials of particular significance discussed in this subsection are succinctly summarized in Table 1 for reader convenience.

SPION-based contrast agents offer exciting possibilities in vascular imaging, particularly in the context of MRA. These agents have been extensively evaluated for enhancing MRA, with early studies showcasing their effectiveness in visualizing pulmonary and venous systems, detecting arterial thrombosis, and highlighting aortic stent-graft endoleaks. The prolonged blood circulation time of some SPION formulations has been harnessed to improve MRA image acquisition. Clinical phase I trials have shown promise in coronary artery imaging, although challenges related to imaging time and spatial resolution remain. Novel SPION formulations continue to enhance vascular imaging, yielding valuable insights into various vascular pathologies and contributing to our understanding of neurodegenerative diseases.

4.3 Cell tracking

Over the past few years, cell and gene therapies have gained increasing popularity and have proven to be more effective, resulting in 27 approvals from FDA by December 2022. A significant challenge in gaining approval for clinical use of cell-based treatments is the complexity of assessing and pinpointing the specific impact of each mechanism that adult stem cells employ for tissue regeneration.[78] When transplanted, mesenchymal stem cells (MSCs) can travel to the site of injury and facilitate tissue regeneration, primarily by delivering trophic and paracrine factors, for example in cerebral infarction.

MRI cell tracking emerged as a novel approach in 1993[79] in order to examine cell survival and migration following grafting. A groundbreaking study in 2002[80] was the first to explore cell tracking for brain injury repair, marking a significant milestone in the evaluation of treatment outcomes.

Numerous other studies over the last two decades restated SPION's reliable tracking abilities by labeling MSCs. Amsalem *et al.*[81] tracked MSCs injected into groups of rats that had suffered a myocardial infarction, while Chapon *et al.*[82] compared MRI imaging with PET results, confirming the homing of the NPs to the injured site for up to 6 weeks after. Lee *et al.*[83] tracked MSCs labeled with ferumoxytol that were introduced through stereotactic injection into the hippocampi of a transgenic mouse model with familial Alzheimer's disease for 14 days, demonstrating the effectiveness of this approach. Ferumoxytol was again tested by Hamilton *et al.*[84] in 2019 in a mouse model of osteoarthritis, where it helped showing the anti-inflammatory characteristics of labeled MSCs on synovial inflammation following intra-articular injection.

Yan *et al.*[85] used magnetically targeted iron oxide@polydopamine-labeled human umbilical cord mesenchymal stem cells to reduce the area of infarcted cerebral tissue and facilitate microglial shift to a neuroprotective and pro-neuroinflammative phenotype. Similar particles were used by Duan *et al.*[86] in 2020 in the treatment of femoral head osteonecrosis, optimizing tissue repair ability, while Li *et al.*[87] used Fe_3O_4@polydopamine NPs as a therapeutic strategy for burn wound healing.

Furthermore, SPION seem to enhance adipogenesis and osteogenesis by their presence alone[88,89] or in the presence of a magnetic field.[90]

Li *et al.*[91] showed in 2019 that SPION facilitate the movement of mesenchymal stem cells toward sites of injury while having no negative effects on their properties; however, Kolecka *et al.*[92]

Table 1 Clinical Trial investigations for vascular imaging

Contrast agent	Dose	Condition	NCT number/approved by	Phase	Status	Ref.
Citrate-coated very small SPIONs	Cohort 1 : 1.1, cohort 2 : 2.2, cohort 3 : 2.5, cohort 4 : 3.3 (mg iron per kg of bodyweight)	Coronary artery disease	Local Ethics Committee	1, 2	Completed	63
Ferumoxytol	—	Coronary artery disease	NCT02954510	3	Ongoing	65
Ferumoxytol	Single dose, 510 mg	Reduced kidney function	Mass General Brigham Institutional Review Board	—	Completed 2018	72
Domestic polysaccharide SPIONs	—	Chronic kidney diseases	NCT05045872	1	Ongoing	74
Ferumoxtran-10	2.6 mg iron per kg of bodyweight	Reduced kidney function	Local Ethics Institutional Review Board	—	Completed	71
Ferumoxytol	4 mg per kg of bodyweight	Ischemic stroke	South East Scotland Research Ethics Committee (14/SS/1081)	—	Completed	68

Open Access Article. Published on 02 4 2024. Downloaded on 2024-08-05 11:52:04.
This article is licensed under a Creative Commons Attribution 3.0 Unported Licence.

showed a potential negative effect on chondrogenesis, using Endorem in a canine model while successfully tracking adipose stem cells.

Leveraging MSCs for targeted gene therapy and NPs-assisted tracking offers innovative solutions in clinical oncology. Noninvasive MRI, aided by SPION, enhances precision in tracking therapeutic MSCs, by leveraging their intrinsic tumor-seeking properties[93] (Fig. 5). Sca-1 positive bone marrow cells, magnetically labeled, were tracked using serial MRI in tumor-bearing mice, revealing dark regions within and around tumors on days 4, 9, and 11, indicating incorporation of labeled cells into tumor vasculature and parenchyma. By day 11, a dark rim appeared at the tumor's periphery, confirmed by *ex vivo* gradient images, suggesting neovascularization primarily occurs there in later tumor stages. Hsu *et al.*[94] developed in 2019 a state-of-the-art theranostic technique for MRI real-time tracking of the tumor infiltration of therapeutic stem cells, namely polyethylene glycol-coated superparamagnetic iron oxide-labelled placenta-derived mesenchymal stem cells, in a mouse model of glioblastoma. Hunger *et al.* tracked T-cells by labeling them with SPION in order to monitor T-cell activation immunotherapies against glioma.[95]

SPIONs have demonstrated their reliability in tracking MSCs, supporting research in various conditions such as myocardial infarction, Alzheimer's disease, and osteoarthritis. Additionally, SPIONs show promise in promoting tissue regeneration. To fully harness the potential of stem cell therapies and ensure their effectiveness, it is imperative to develop techniques for comprehensively understanding the biodistribution and fate of administered cells. MRI cell tracking, particularly when employing SPIONs, holds substantial potential for advancing cell-based treatments and personalized medicine.

4.4 Lymph node imaging

Lymph node staging is paramount for choosing the right therapeutic strategy in any type of cancer and can predict patient survival time. In practice, we have imaging options that include ultrasound and non-contrast-enhanced CT or MRI and surgical options consisting of lymph node removal and histological interpretation. Imaging lymph nodes relies on the assessment of changes in size and morphology only, resulting in a low sensitivity and an even lower specificity, especially when compared to USPIO-enhanced MR imaging. PET managed to surmount some of these drawbacks but is still constrained by its resolution limit.[96] Surgical intervention is invasive, prone to complications and only studies the perilesional area, which often leads to an underestimation of metastasis by missing far-

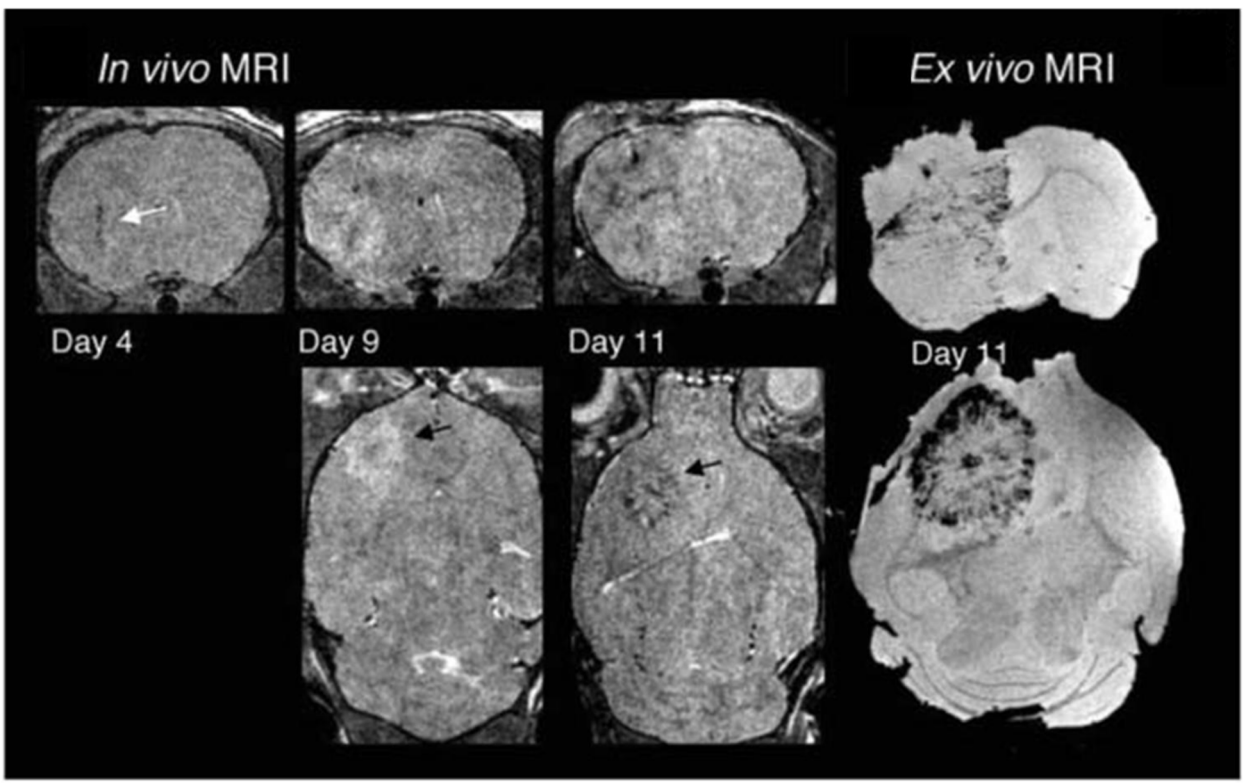

Fig. 5 Targeting tumor vasculature, Sca-1 positive bone marrow cells, magnetically labeled, were tracked using serial MRI in tumor-bearing mice. Three-dimensional RARE images acquired on days 4, 9, and 11 revealed dark regions emerging within and around the tumors, signifying the incorporation of labeled cells into both tumor vasculature and parenchyma. By day 11, a dark rim became evident at the tumor's periphery. Corresponding *ex vivo* gradient images on day 11 confirmed MR evidence of labeled cell incorporation, indicating that neovascularization primarily occurs at the tumor periphery in later stages of tumor development. Modified with permission from Tang, C. *et al.* (2010)[93] Creative Commons – Attribution 2.5 Generic (https://creativecommons.org/licenses/by/2.5/).

 © 2024 The Author(s). Published by the Royal Society of Chemistry

Open Access Article. Published on 02 4 2024. Downloaded on 2024-08-05 11:52:04.
This article is licensed under a Creative Commons Attribution 3.0 Unported Licence.

away ones, especially in the pararenal and internal iliac region. Moreover, the two techniques cannot detect very small lymph nodes, which can be metastatic too.

USPIOs with a hydrodynamic diameter of 20–30 nm and a dextran coating have a long blood circulation time, making them suitable for MR lymphography. Over time, USPIOs that extravasate into tissues are collected in the lymphatic system and ingested by lymph node macrophages. This process decreases the signal intensity in T_2 and T_2^*-weighted MR imaging while increasing the T_1 signal. Metastatic lymph nodes, which often have a reduced number and function of macrophages, lead to lower USPIO uptake and subsequent signal modification. This can serve as an indirect method to diagnose metastatic lymph nodes, particularly those that are remote or small. Further studies showed that GRE T_2^*-weighted sequence showed the best nodal characterisation compared to fast spin-echo T_2-weighted ones, the latter being useful for anatomic localization.[97] This technique has been demonstrated in clinical trials for several malignancies (Fig. 6), including head and neck,[98] breast,[99] lung,[100] esophagus,[101] stomach,[102] rectum,[103] gynecological,[104] bladder and prostate cancers.[105]

Ferumoxtran (Combidex® (USA), Sinerem® (EU)) and ferumoxytol (Feraheme® (USA), Rienso® (EU)) have been in clinical trials for lymph node imaging but didn't make it into practice. For example, Sinerem had its application removed by Guerbet from European Medicines Agency in 2007 in a phase 3 study due to the not definitely proven specificity of lymph node detection in pelvic carcinoma patients. Feraheme was already approved for anemia therapy as iron replacement, and was used off-label as a replacement for Combidex. Unfortunately, in 2015 FDA issued a "Boxed Warning" regarding serious risks of fatal anaphylaxis and furthermore the nodal contrast between benign and malignant was less prominent even with triple dose of feraheme, compared to Combidex.[106]

Ferumoxtran gained new-found interest in 2013 when the Radboud University Medical Center in The Netherlands started the process of producing Combidex under the same specifications as previously described, to use especially in the setting of prostate cancer.[107] A meta-analysis by Woo *et al.* in 2018 compared the diagnostic accuracy of MRI in finding pelvic lymph node metastasis in patients with prostate and bladder cancer between 1980–2003 and 2000–2017, finding an improved sensitivity (0.39 to 0.56) and specificity (0.82 to 0.94) and attributing the effect to the use of USPIOs. Nevertheless, the sensitivity is still poor and a negative USPIO-MRI examination does not rule out the requirement of surgery.[108] A lot of research is carried out in Nijmegen by Professor Tom Scheenen and his team, with mixed results. When comparing Gadolinium-Prostate Specific Membrane Antigen (Ga-PSMA) PET/CT with ferumoxtran-10 NP-enhanced MRI in prostate cancer lymph node assessment, both modalities identified suspicious lymph nodes that were unnoticed by the other, with the latter proving better in detecting smaller suspicious lymph nodes, suggesting a complementary role.[109] An ongoing phase 3 trial[110] is putting ferumoxtran-10's ability to the test against unenhanced MRI. When evaluating lymph nodes in rectal cancer, USPIO-enhanced MRI was not able to differentiate between small inflammatory *versus* metastatic nodes *in vivo* on a 3T machine, warranting improvements in order to correlate smaller lymph nodes to histopathological findings.[111] FerroTrace and Indocyanine Green are being used in a phase 1 and 2 trial[112] for sentinel lymph node mapping in colorectal cancer. They also developed a new reading algorithm for discerning benign from malignant lymph nodes in head and neck cancer patients.[113] Peter Choyke[114] and his team studied the detection of lymph nodes by ferumoxytol-enhanced MR lymphography in genito-urinary malignancies, yielding promising results with a high sensitivity of 98.0% but an average specificity of 64.4%.[115] To overcome these challenges a few methods are trying to be employed. The use of a 7T MRI system can improve the intrinsic signal-to-noise ratio and, moreover, can further decrease the T_2^* signal after USPIO uptake because of increased susceptibility effects.[116] Research done by He and Wei in 2016 claim diffusion-weighted sequences can have a role in discerning benign and malignant lymph nodes in cervical cancer, showing statistically significant differences in ADC values, granting a high specificity but a low sensitivity to the technique.[117] Further research is needed in these areas.

Sentinel lymph node status is pivotal in both breast and skin cancer patients. Great strides are undertaken to find a minimally-invasive technique for accurately assessing them and sack the gold standard of axillary lymph node dissection. Motomura *et al.* have showed that sentinel lymph node status can be predicted using SPION-enhanced MRI with a low dose of ferucarbotran (Resovist) with the incorporation of a fat-suppression sequence with a sensitivity of 100% and specificity of 96%, being able to detect micro metastasis as small as 1.7 mm.[118] They also proved equivalent accuracy of the technique on 1.5T machines.[119] These studies were used as a background in the MAGMEN feasibility study, which correctly predicted some of the metastasis of extremity melanoma using a low-dose SPIONs injected subcutaneously.[120] Karakatsanis *et al.* developed another technique for minimally invasive axillary mapping; in a phase 2 trial published in 2021, by integrating SPION-enhanced MR lymphography with Magnetic-guided Axillary UltraSound (MagUS) and biopsy, providing comparable results with axillary lymph node dissection[121] (Fig. 7). The clinical trials highlighted in this subsection, which stand out in terms of relevance and representativeness, are consolidated in Table 2 for easy reference.

In summary, lymph node staging is of utmost importance in cancer diagnosis and treatment planning. Existing methods such as ultrasound, non-contrast-enhanced CT or MRI, and surgical interventions have their limitations in terms of sensitivity and specificity. Iron oxide NPs-enhanced MR imaging has emerged as a promising tool to overcome these limitations, allowing for the detection of metastatic lymph nodes, especially small or distant ones. Clinical trials have demonstrated the potential of USPIOs like ferumoxtran and feraheme in various malignancies. However, challenges remain, and ongoing research aims to enhance the accuracy and applicability of this technique, including exploring higher magnetic field strengths, diffusion-weighted sequences, and innovative approaches for sentinel lymph node assessment. These developments signify

Open Access Article. Published on 02 4 2024. Downloaded on 2024-08-05 11:52:04.
This article is licensed under a Creative Commons Attribution 3.0 Unported Licence.

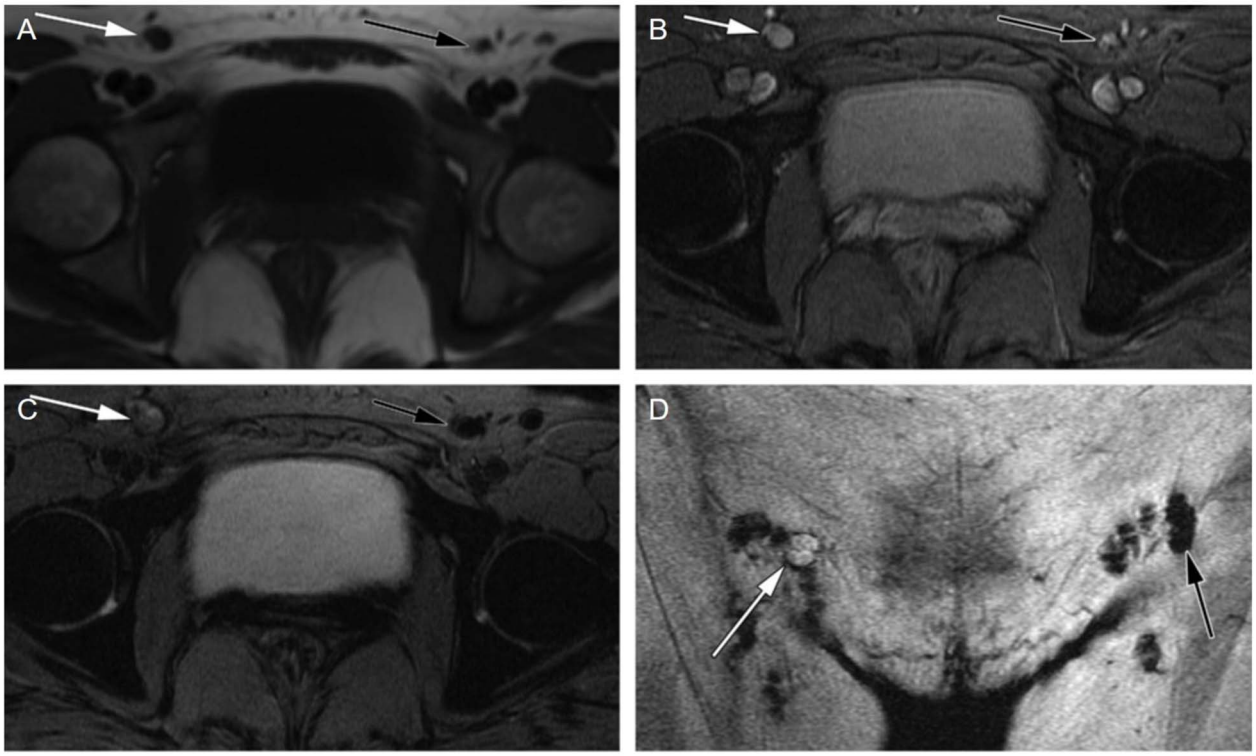

Fig. 6 Case of a malignant inguinal node in a 47 year-old patient with vulvar cancer. The axial precontrast T_1-weighted GRE image (A) reveals a borderline enlargement of the right inguinal node (white arrow) compared to the left inguinal node (black arrow). In the axial precontrast T_2^*-weighted GRE image (B), both inguinal nodes (arrows) appear bright. Following contrast administration, the axial postcontrast T_2^*-weighted GRE image (C) demonstrates that the right inguinal node (white arrow) remains bright, while the left inguinal node becomes dark (black arrow). Additionally, the coronal post contrast T_2^*-weighted GRE image (D) provides valuable information for surgical planning, illustrating the relationship of the nodes to the inguinal fold. These imaging characteristics are indicative of a malignant right inguinal node in MR lymphography, a diagnosis that was subsequently confirmed through histologic analysis, while the left inguinal node was found to be benign. The recommended USPIO dose of 2.6 mg kg^{-1} is diluted in 100 ml of normal saline and infused over 30 minutes. Copyright (2009), with permission from Radiological Society of North America.[104]

a significant step forward in improving lymph node staging and, consequently, patient care across different cancer types.

4.5 Tumour imaging

Tumor detection using SPION relies on three primary mechanisms.[125] Firstly, upon introduction into the bloodstream, SPIONs are swiftly sequestered by macrophages within the Mononuclear Phagocyte System (MPS), spanning the liver, spleen, lymph nodes, and bone marrow. Secondly, the EPR effect takes center stage in solid tumors, where the abnormal angiogenesis results in larger vessel pores (100+ nm),[126] facilitating the infiltration of SPIONs into the tumor tissue. Lastly, active targeting strategies involve customizing SPIONs with ligands that bind to specific tumor markers, such as folate receptors, transferrin receptors, and epidermal growth factor receptors on cancer cells[127,128]. This targeted approach combines the passive EPR-based accumulation with active binding to tumor markers, although its efficacy remains a subject of ongoing debate. As thousands of recently published research papers suggest, the EPR effect is very heterogeneous in humans,[129] varying according to tumor type, location, blood perfusion and the properties of the chemotherapeutic agents.[130]

Wang *et al.*'s study[131] introduces a method to enhance the delivery and distribution of ultrafine SPION (under 5 nm) within tumors by fully taking advantage of the EPR effect. These ultrafine SPION can easily exit blood vessels and penetrate tumor tissue due to their small size, then cluster in the tumor's acidic environment to prevent re-entering the bloodstream. *In vivo* imaging showed initial "bright" T_1 contrast in tumor blood vessels and surroundings in the first hour, shifting to "dark" T_2 contrast within the tumor after 24 h, indicating cluster formation in the tumor's interstitial space.

In the liver, uptake by the Kupffer cells (the autochthonous macrophages) lets us achieve the contrast needed, owing to the fact that primary or secondary liver malignancies do not express Kupffer cells. In T_2-weighted images, the presence of SPIONs in normal liver tissue results in a dark appearance, while the liver tumor remains conspicuously bright. This distinction arises from the reduced accumulation of SPION in the tumor due to its lower phagocytic activity.

Liver imaging was the application for the first NP-based iron oxide contrast agent approved by the FDA (ferumoxide) and also for the later developed ferucarbotran. They were used in clinical practice to discriminate between malignant (hepatocarcinoma

 © 2024 The Author(s). Published by the Royal Society of Chemistry

Open Access Article. Published on 02 4 2024. Downloaded on 2024-08-05 11:52:04.
This article is licensed under a Creative Commons Attribution 3.0 Unported Licence.

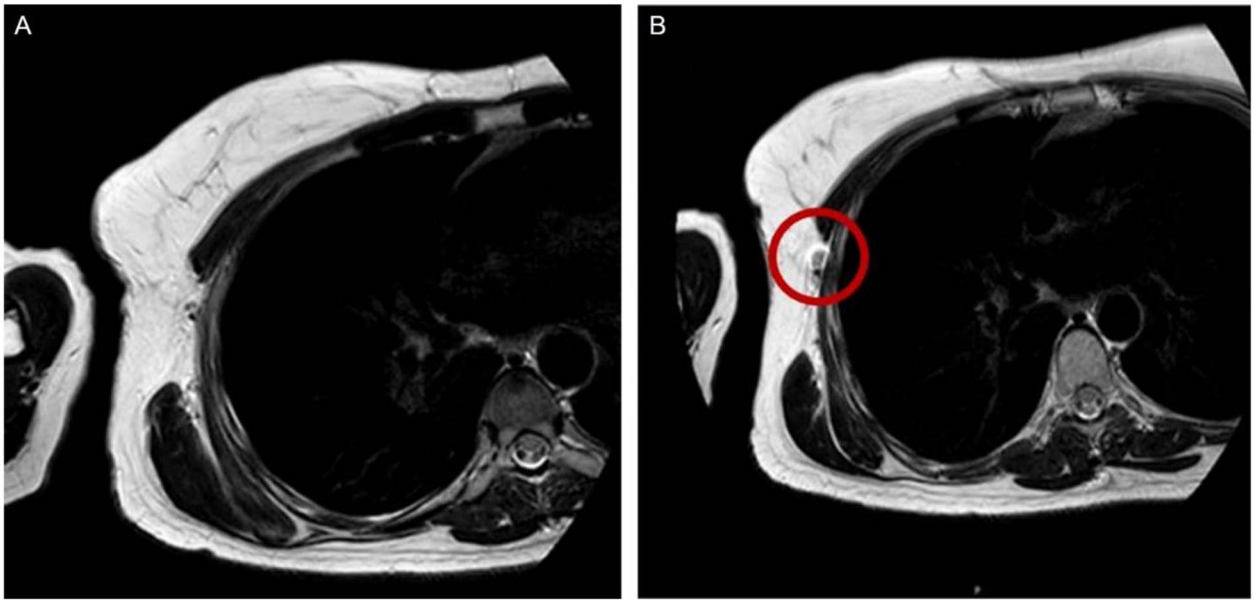

Fig. 7 (A and B) Illustrates the visualization of the sentinel lymph node with MRI both before and after the administration of SPIO. Enhancement of the sentinel lymph node becomes apparent following the injection of SPIO, as highlighted by the red circle. Redistributed with permission from Jazrawi, A. *et al.*, (2021)[122] Creative Commons – Attribution 4.0 International – CC BY 4.0 (https://creativecommons.org/licenses/by/4.0/).

and metastasis) and benign (adenoma, hemangioma, focal nodular hyperplasia) hepatic lesions[132,133] (Fig. 8). The two compounds were compared with each other by Chen *et al.* and no significant difference was found in T_2-weighted signal intensities or contrast-to-noise ratio.[134]

Meanwhile, these two contrast agents have been withdrawn from the market (except ferucarbotran in Japan), citing multiple reasons. One specific problem was the inability to differentiate normal liver from a well-differentiated hepatocellular carcinoma, which contains high amounts of macrophages. Gadolinium-based contrast agents are uptaken by hepatocytes instead of macrophages so they don't exhibit this limitation.[135] SPIONs can still be a safe alternative for discerning liver lesions in the setting of limited kidney function (glomerular filtration

Table 2 Clinical Trial investigations for lymph node imaging

Contrast agent	Dose	Primary cancer type	NCT number/approved by	Phase	Status	Ref.
FerroTrace	—	Colorectal	NCT05092750	1, 2	Completed 2023	112
Ferucarbotran	Single dose, 6 ml	Breast	Osaka Medical Centre for Cancer and Cardiovascular Diseases Review Border	—	Completed 2016	118
MagTrace	Single dose, 2 ml	Breast	Regional Ethics Board in Uppsala (DNR 2016 – 385)	2	Completed 2021	121
Iron oxide crystalline NPs covered wtih dextran	2.6 mg iron per kg of bodyweight	Oesophageal	Medical Ethical Committee of the University Medical Center Groningen	—	Completed 2009	101
Low-molecular weight, iron oxide coated with dextran	2.6 mg iron per kg of bodyweight	Rectal	—	—	Completed 2006	103
Ferumoxytol	Cohort 1 : 4, cohort 2 : 6, cohort 3 : 7.5 (mg iron per kg of bodyweight)	Prostate	Review Board of National Institutes of Health, Bethesda	1	Completed 2012	107
Ferumoxtran-10	2.6 mg iron per kg of bodyweight	Prostate	NCT04261777	3	Ongoing	110
Ferumoxtran-10	2.6 mg iron per kg of bodyweight	Head and neck squamous cell carcinoma	NCT03817307	—	Ongoing	113 and 123
MagTrace	Cohort 1 : 5.6–14, cohort 2:2.8–3.4, cohort 3 : 0.6–1.4 (mg iron per kg of bodyweight)	Melanoma	NCT03898687	1	Completed 2020	120 and 124

Open Access Article. Published on 02 4 2024. Downloaded on 2024-08-05 11:52:04.
This article is licensed under a Creative Commons Attribution 3.0 Unported Licence.

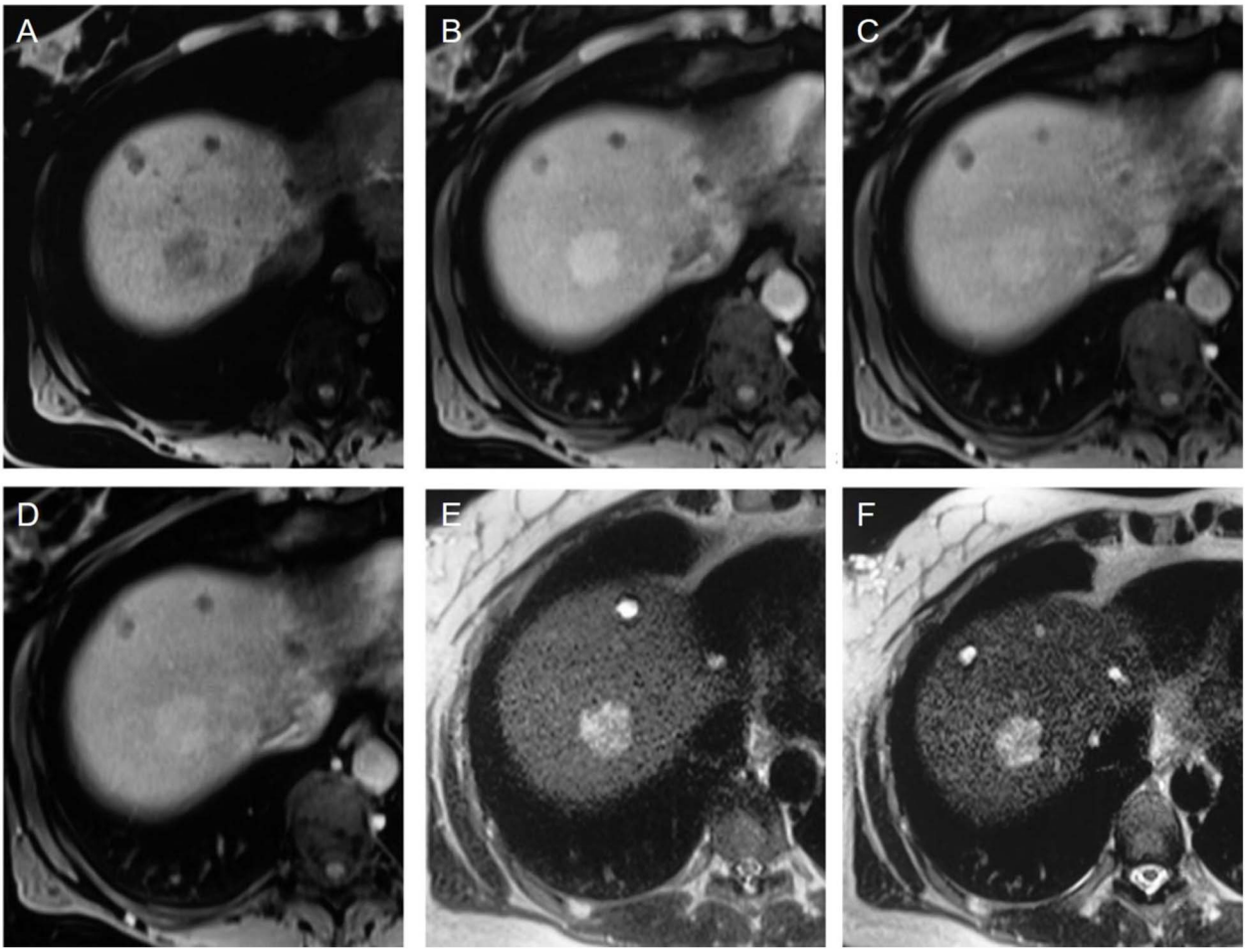

Fig. 8 (A–F) Showcases of hepatic adenoma. In the unenhanced T_1-weighted VIBE image (A), a nodule is visible, displaying heterogeneous hypointensity in comparison to the surrounding right liver lobe tissue. Following the slow bolus administration of Resovist, the nodule undergoes enhancement in the arterial phase (B) without significant wash-out during the portal venous (C) and equilibrium phases (D). On the unenhanced HASTE T_2-weighted sequence (E), the lesion appears hyperintense compared to the liver parenchyma, with no significant alterations noted in the 10 minutes contrast-enhanced acquisition (F) upon visual assessment. However, quantitative analysis reveals a 33% signal loss in the nodule, which still appears hyperintense due to a 53% signal loss in the surrounding parenchyma. It's important to note that all the images (A–F) exhibit small cysts in the anterior portion of the liver parenchyma. Copyright (2009), with permission from John Wiley and Sons.[132]

rate < 30 ml min^{-1} per 1.73 m^2) or just wishing to avoid nephropathy and the risk of nephrogenic systemic fibrosis.[69]

Similar to the liver, SPION accrue in the spleen, allowing the detection of metastasis and the rare spleen primary malignancies.[136] Further uses encompass the detection and separation of heterotopic splenic tissue, particularly accessory spleens or splenosis. Accessory spleens are a common finding but can pose diagnostic difficulties when located intrapancreatically and need to be differentiated from pancreatic cancer. Splenosis is a benign entity, with the greatest importance being the need to distinguish them from more sinister pathology.

Contrast-enhanced MRI is commonly used to visualize brain tumors and assess BBB integrity. However, when compared to Gd-based agents, ferumoxytol did not demonstrate superiority in detecting brain cancer lesions with contrast-enhanced MRI.[137] The advantage of SPIONs and USPIOs over small molecule Gd chelates lies in their much lower extravasation rate into the extravascular extracellular space. This characteristic enables a more precise determination of the relative cerebral blood volume (rCBV), leading to improved visualization and quantification of tumor vascularization. In the case of glioblastoma multiform for example, this is needed because distinguishing between real tumor progression and pseudo progression (treatment-induced inflammation with BBB integrity loss) is crucial for treatment monitoring. Gahramanov *et al.*[138] put this to test in 2013 and showed that ferumoxytol can make this distinction, being a good prognostic biomarker and, unlike gadoteridol, does not require contrast agent leakage correction. Furthermore, recent concerns about neuronal tissue deposition of Gd in patients with normal renal function[139] warrant additional studies.

Tumor macrophage content plays a substantial role in tumor angiogenesis, progression, metastasis and response to treatment. Ferumoxytol-enhanced MRI offers the first non-invasive technique clinically available for this measurement, demonstrated for high-grade gliomas by Iv *et al.*[140] in a pilot study in

 © 2024 The Author(s). Published by the Royal Society of Chemistry

Open Access Article. Published on 02 4 2024. Downloaded on 2024-08-05 11:52:04.
This article is licensed under a Creative Commons Attribution 3.0 Unported Licence.

2019, where contrast enhancement correlated with iron-containing macrophages concentration.

Ghorbani *et al.*[141] developed two nanoprobes suitable as negative contrast agents for the molecular imaging of prostate cancer.

Driven by the global imperative to combat cancer, recent years have witnessed a profound expansion in oncology research, particularly emphasizing the vast potential of SPIONs. Unlike the traditional FDA-approved compounds, many of the new nanoformulations are groundbreaking, leading to a rich tapestry of results. The core strength of SPIONs lies in their adaptability. They can be tailored with a wide array of coating materials to improve biocompatibility, and functionalised with specific targeting molecules, ensuring pinpoint accuracy to desired regions, such as cancer cells.

In breast cancer detection, formulations currently under scrutiny include SPION coated with porphyrin and functionalized with trastuzumab[142] or SPION nanoworms conjugated with Indocyanine Green.[145] Important research is being conducted in regard to triple-negative breast cancer, where Wu *et al.*[144] used hybrid iron oxide–gold NPs functionalized with the Hsp70 peptide TPP *via* a PEG4 linker in order to target tumor-specific membrane Hsp70 and significantly sensitize tumor cells against radiation therapy. Early diagnosis of hepatocellular carcinoma is crucial; a phase II clinical trial[145] conducted by Chiang *et al.*[145] tested a newly developed SPIO in the form of iron oxide nano-particle m-PEG-silane injection, yielding this technique as safe and efficacious. Another clinical study by Hama *et al.*[146] was able to detect every hepatic malignancy in a 0.35T MRI machine. Regarding prostate cancer, prostate-specific membrane antigen (PSMA) has emerged as the best theranostic target,[147] warranting multiple studies that used active targeting in the form of antibodies[148] or even an innovative PSMA-targeting Glu-Urea-Lys scaffold.[149] Martin *et al.*[150] targeted claudin-3 and -4 using a non-toxic *Clostridium perfringens* enterotoxin, showing overexpression in high grade prostate cancers. The overexpression of folate receptor alpha in the majority of ovarian malignancies have led to the development of anti-folate receptor alpha SPIONs that can reliably detect ovarian tumors.[151] Lung tumors can also be visualised by taking advantage of the overexpressed folate receptor, as Kimura *et al.*[152] showed by using polyethylene glycol-coated and dextran-coated SPIONs. Furthermore, using a hipoxia-sensitive metronidazole moiety, Yang *et al.*[153] was able to accurately measure hipoxia in lung tumors using T_1-weighted sequences, predicting tumor development. Furthermore, ongoing clinical trials are using SPION to study the tumor infiltration of glioblastoma,[154] to assess functionally active liver parenchyma after liver cancers[155] or to stage bladder cancer.[156]

Nevertheless, a predominant proportion of studies leveraging the tumor-imaging potential of magnetic NPs predominantly consist of theranostic platforms. Within these platforms, the inherent imaging attributes of magnetic NPs are coupled with various therapeutic strategies, thereby synergistically contributing to the mitigation of the pathological condition. This is the case in a vast array of diseases where clinical and preclinical studies are underway and magnetic NPs show a great deal of promise: brain cancer, especially gliomas,[157–159] breast cancer,[160,161] prostate cancer,[162,163] ovarian cancer,[164,165] cervical cancer,[166–168] bladder cancer,[169–172] lung cancer,[173] liver cancer[174] and even skin cancer.[175–177] The subject of theranostic platforms and other advances of magnetic NPs will be discussed in the following section of this paper.

In summary, SPIONs are a promising tool for tumor detection in MRI. Recent research has explored ultrafine SPIONs, which can enhance tumor delivery and distribution by capitalizing on the EPR effect. They have been valuable in liver and spleen imaging, aiding in the differentiation of lesions. While some SPION-based contrast agents have been withdrawn from the market due to challenges in distinguishing liver lesions, they remain a suitable option for patients with kidney function concerns. In brain tumor imaging, SPIONs offer advantages in determining rCBV. While oncology remains a prime focus due to its pressing global significance, the versatility and advantages of SPIONs transcend this field. Their potential applicability spans across various medical domains, broadening their potential applications.

5. Beyond imaging: expanding horizons of magnetic nanoparticles applications

Magnetic NPs have not only demonstrated superior results in MRI compared to traditional contrast agents but their potential appears boundless, offering manifold benefits beyond current applications. While initial research predominantly honed in on their use in MRI, it's evident that we are merely at the inception of uncovering their full spectrum of capabilities in the realm of medical imaging.

At the forefront of imaging advancements stands Magnetic Particle Imaging (MPI) – a cutting-edge, non-invasive imaging technique that capitalizes on SPION, reminiscent of those utilized in MRI. Distinguished by its unique physical principles of not presenting background noise, MPI can produce optimal image contrast similar to PET/SPECT investigations, but without the irradiation. This characteristic sets it apart from MRI and positions MPI as a superior choice for quantitative determinations.

In addition, due to their facile functionalization, magnetic NPs hold a great promise for developing formulations that can be used for multimodal imaging. Their versatility allows for their integration into various imaging techniques, like CT, PET/SPECT, ultrasound, fluoroscopy or photoacoustic imaging.[178]

Especially in the oncology field, SPION have proven to be an extremely versatile compound and have been used as part of theranostic platforms employing a variety of strategies, from drug delivery to magnetic hyperthermia and the newly discovered ferroptosis. Ferroptosis is characterized by substantial iron accumulation that leads to diminished antioxidant capacity and an uptick in lipid reactive oxygen species within cells, culminating in oxidative cell death. Advancements in the field have culminated in the introduction into clinical use of a theranostic system, the Nanotherm formulation,[179] that have gained FDA

Open Access Article. Published on 02 4 2024. Downloaded on 2024-08-05 11:52:04.
This article is licensed under a Creative Commons Attribution 3.0 Unported Licence.

and European Medicines Agency (EMA) approvals for cancer treatment through hyperthermia. This innovative approach is currently applied in the management of conditions such as brain, prostate, and pancreatic cancers.

Given the inherent versatility and adaptability of SPIONs, the possibilities for tailoring them to specific medical needs and therapeutic strategies are virtually limitless. By integrating coating materials, fluorophores, drugs, and other active molecules, we can precisely craft them to address individual conditions and treatments, pushing the boundaries of personalized medicine and medical imaging.

6. Conclusion

The multifaceted world of medical imaging is experiencing a transformative era, largely driven by the advancements in nanotechnology. As elaborated in this paper, MRI stands as an invaluable tool, particularly for soft tissue analysis, due to its non-invasiveness, absence of ionizing radiation, and superior spatial resolution. Gadolinium-based NPs, which have historically been at the forefront of MRI contrast agents, have paved the way for a clearer understanding of various medical conditions. However, emerging evidence of their potential toxicity and limitations highlights the pressing need for alternative contrast agents.

Consequently, the focus has notably shifted to SPIONs due to their safety profile and customizable nature. Their ability to alter both T_1 and T_2 relaxation times, combined with their superparamagnetic capabilities, sets them apart. What distinguishes SPIONs from their therapeutic contemporaries is their intrinsic malleability. Their structural and functional properties can be meticulously tailored to incorporate a variety of coatings, enhancing their biocompatibility with the human system. Furthermore, by functionalizing them with specific targeting molecules, we are effectively crafting microscopic guided missiles, directing them to their intended destinations.

The versatility of SPIONs is evident from their expanding role in clinical settings. Whether it's characterizing liver lesions, tracking macrophages in inflammation and infection processes, or assessing atherosclerotic plaque stability, SPIONs have demonstrated exceptional promise. In the fight against cancer, their adaptability to be tailored with specific targeting molecules ensures that they're not just limited to imaging but can also play a pivotal role in theranostic platforms, combining diagnostic and therapeutic applications.

However, as with all advancements, challenges persist. While certain SPION formulations face drawbacks like inadequate renal clearance or potential side effects from iron overload, ongoing research and clinical trials are working relentlessly to circumvent these challenges and harness their full potential.

To encapsulate, the horizon of medical imaging, especially MRI, is vast and continually expanding. In this evolving landscape, departing from the confines of traditional FDA-approved compounds, the aforementioned avant-garde nanoformulations are establishing new frontiers in diagnostics and therapeutics. Our endeavor remains to continually innovate and optimize, ensuring the best patient outcomes while minimizing risks. The journey of exploration in the realm of nanotechnology and medical imaging is vast and ongoing, and the forthcoming chapters promise further exciting revelations and solutions.

Conflicts of interest

There are no conflicts of interest to declare.

Acknowledgements

Raluca Borlan is thankful for the 'Grant for young scientists', awarded by Babes-Bolyai University, contract number SRG-UBB 32995/23.06.2023.

References

1 O. S. Faragallah, H. El-Hoseny, W. El-Shafai, W. A. El-Rahman, H. S. El-Sayed, E.-S. M. El-Rabaie, F. E. A. El-Samie and G. G. N. Geweid, A Comprehensive Survey Analysis for Present Solutions of Medical Image Fusion and Future Directions, *IEEE Access*, 2021, **9**, 11358–11371, DOI: 10.1109/ACCESS.2020.3048315.

2 S. Hussain, I. Mubeen, N. Ullah, S. S. U. D. Shah, B. A. Khan, M. Zahoor, R. Ullah, F. A. Khan and M. A. Sultan, Modern Diagnostic Imaging Technique Applications and Risk Factors in the Medical Field: A Review, *BioMed Res. Int.*, 2022, **2022**, 1–19, DOI: 10.1155/2022/5164970.

3 G. Kandasamy and D. Maity, Recent advances in superparamagnetic iron oxide nanoparticles (SPIONs) for *in vitro* and *in vivo* cancer nanotheranostics, *Int. J. Pharm.*, 2015, **496**, 191–218, DOI: 10.1016/j.ijpharm.2015.10.058.

4 Z. Zhou, R. Bai, J. Munasinghe, Z. Shen, L. Nie and X. Chen, T_1–T_2 Dual-Modal Magnetic Resonance Imaging: From Molecular Basis to Contrast Agents, *ACS Nano*, 2017, **11**, 5227–5232, DOI: 10.1021/acsnano.7b03075.

5 H. B. Harvey, V. Gowda and G. Cheng, Gadolinium Deposition Disease: A New Risk Management Threat, *J. Am. Coll. Radiol.*, 2020, **17**, 546–550, DOI: 10.1016/j.jacr.2019.11.009.

6 I. Fernández-Barahona, M. Muñoz-Hernando, J. Ruiz-Cabello, F. Herranz and J. Pellico, Iron Oxide Nanoparticles: An Alternative for Positive Contrast in Magnetic Resonance Imaging, *Inorganics*, 2020, **8**, 28, DOI: 10.3390/inorganics8040028.

7 A. Shariati, T. Ebrahimi, P. Babadinia, F. S. Shariati and R. Ahangari Cohan, Synthesis and characterization of Gd^{3+}-loaded hyaluronic acid-polydopamine nanoparticles as a dual contrast agent for CT and MRI scans, *Sci. Rep.*, 2023, **13**, 4520, DOI: 10.1038/s41598-023-31252-0.

8 G. B. Toth, C. G. Varallyay, A. Horvath, M. R. Bashir, P. L. Choyke, H. E. Daldrup-Link, E. Dosa, J. P. Finn, S. Gahramanov, M. Harisinghani, I. Macdougall, A. Neuwelt, S. S. Vasanawala, P. Ambady, R. Barajas, J. S. Cetas, J. Ciporen, T. J. DeLoughery, N. D. Doolittle, R. Fu, J. Grinstead, A. R. Guimaraes, B. E. Hamilton, X. Li,

 © 2024 The Author(s). Published by the Royal Society of Chemistry

Open Access Article. Published on 02 4 2024. Downloaded on 2024-08-05 11:52:04.
This article is licensed under a Creative Commons Attribution 3.0 Unported Licence.

H. L. McConnell, L. L. Muldoon, G. Nesbit, J. P. Netto, D. Petterson, W. D. Rooney, D. Schwartz, L. Szidonya and E. A. Neuwelt, Current and potential imaging applications of ferumoxytol for magnetic resonance imaging, *Kidney Int.*, 2017, **92**, 47–66, DOI: 10.1016/j.kint.2016.12.037.

9 F. N. Sayed and V. Polshettiwar, Facile and Sustainable Synthesis of Shaped Iron Oxide Nanoparticles: Effect of Iron Precursor Salts on the Shapes of Iron Oxides, *Sci. Rep.*, 2015, **5**, 9733, DOI: 10.1038/srep09733.

10 B. R. Smith, P. Kempen, D. Bouley, A. Xu, Z. Liu, N. Melosh, H. Dai, R. Sinclair and S. S. Gambhir, Shape Matters: Intravital Microscopy Reveals Surprising Geometrical Dependence for Nanoparticles in Tumor Models of Extravasation, *Nano Lett.*, 2012, **12**, 3369–3377, DOI: 10.1021/nl204175t.

11 D. J. Korchinski, M. Taha, R. Yang, N. Nathoo and J. F. Dunn, Iron Oxide as an Mri Contrast Agent for Cell Tracking: Supplementary Issue, *Magn. Reson. Insights*, 2015, **8**(1), DOI: 10.4137/MRI.S23557.

12 S. J. Dodd, M. Williams, J. P. Suhan, D. S. Williams, A. P. Koretsky and C. Ho, Detection of Single Mammalian Cells by High-Resolution Magnetic Resonance Imaging, *Biophys. J.*, 1999, **76**, 103–109, DOI: 10.1016/S0006-3495(99)77182-1.

13 F. Eibofner, G. Steidle, R. Kehlbach, R. Bantleon and F. Schick, Positive contrast imaging of iron oxide nanoparticles with susceptibility-weighted imaging: Positive Contrast Imaging of SPIO Particles with SWI, *Magn. Reson. Med.*, 2010, **64**, 1027–1038, DOI: 10.1002/mrm.22498.

14 Q. Zhao, J. Langley, S. Lee and W. Liu, Positive contrast technique for the detection and quantification of superparamagnetic iron oxide nanoparticles in MRI, *NMR Biomed.*, 2011, **24**, 464–472, DOI: 10.1002/nbm.1608.

15 E. M. Haacke, S. Mittal, Z. Wu, J. Neelavalli and Y.-C. N. Cheng, Susceptibility-Weighted Imaging: Technical Aspects and Clinical Applications, Part 1, *Am. J. Neuroradiol.*, 2009, **30**, 19–30, DOI: 10.3174/ajnr.A1400.

16 S. Mittal, Z. Wu, J. Neelavalli and E. M. Haacke, Susceptibility-Weighted Imaging: Technical Aspects and Clinical Applications, Part 2, *Am. J. Neuroradiol.*, 2009, **30**, 232–252, DOI: 10.3174/ajnr.A1461.

17 H. Dahnke, W. Liu, D. Herzka, J. A. Frank and T. Schaeffter, Susceptibility gradient mapping (SGM): A new postprocessing method for positive contrast generation applied to superparamagnetic iron oxide particle (SPIO)-labeled cells, *Magn. Reson. Med.*, 2008, **60**, 595–603, DOI: 10.1002/mrm.21478.

18 B. E.-B. Cretu, G. Dodi, A. Shavandi, I. Gardikiotis, I. L. Serban and V. Balan, Imaging Constructs: The Rise of Iron Oxide Nanoparticles, *Molecules*, 2021, **26**, 3437, DOI: 10.3390/molecules26113437.

19 H. Wei, O. T. Bruns, M. G. Kaul, E. C. Hansen, M. Barch, A. Wiśniowska, O. Chen, Y. Chen, N. Li, S. Okada, J. M. Cordero, M. Heine, C. T. Farrar, D. M. Montana, G. Adam, H. Ittrich, A. Jasanoff, P. Nielsen and M. G. Bawendi, Exceedingly small iron oxide nanoparticles as positive MRI contrast agents, *Proc. Natl. Acad. Sci. U. S. A.*, 2017, **114**, 2325–2330, DOI: 10.1073/pnas.1620145114.

20 S. M. Dadfar, K. Roemhild, N. I. Drude, S. von Stillfried, R. Knüchel, F. Kiessling and T. Lammers, Iron oxide nanoparticles: Diagnostic, therapeutic and theranostic applications, *Adv. Drug Delivery Rev.*, 2019, **138**, 302–325, DOI: 10.1016/j.addr.2019.01.005.

21 Y. X. J. Wáng and J.-M. Idée, A comprehensive literature update of clinical researches of superparamagnetic resonance iron oxide nanoparticles for magnetic resonance imaging, *Quant. Imaging Med. Surg.*, 2017, **7**, 88–122, DOI: 10.21037/qims.2017.02.09.

22 B. E.-B. Cretu, G. Dodi, A. Shavandi, I. Gardikiotis, I. L. Serban and V. Balan, Imaging Constructs: The Rise of Iron Oxide Nanoparticles, *Molecules*, 2021, **26**, 3437, DOI: 10.3390/molecules26113437.

23 H. Ittrich, K. Peldschus, N. Raabe, M. Kaul and G. Adam, Superparamagnetic Iron Oxide Nanoparticles in Biomedicine: Applications and Developments in Diagnostics and Therapy, RöFo – Fortschritte Auf Dem Geb. Röntgenstrahlen Bildgeb, *Verfahren*, 2013, **185**, 1149–1166, DOI: 10.1055/s-0033-1335438.

24 D. Rosenblum, N. Joshi, W. Tao, J. M. Karp and D. Peer, Progress and challenges towards targeted delivery of cancer therapeutics, *Nat. Commun.*, 2018, **9**, 1410, DOI: 10.1038/s41467-018-03705-y.

25 M. I. Setyawati, C. Y. Tay, B. H. Bay and D. T. Leong, Gold Nanoparticles Induced Endothelial Leakiness Depends on Particle Size and Endothelial Cell Origin, *ACS Nano*, 2017, **11**, 5020–5030, DOI: 10.1021/acsnano.7b01744.

26 R. Jin, B. Lin, D. Li and H. Ai, Superparamagnetic iron oxide nanoparticles for MR imaging and therapy: design considerations and clinical applications, *Curr. Opin. Pharmacol.*, 2014, **18**, 18–27, DOI: 10.1016/j.coph.2014.08.002.

27 R. A. Trivedi, C. Mallawarachi, J.-M. U-King-Im, M. J. Graves, J. Horsley, M. J. Goddard, A. Brown, L. Wang, P. J. Kirkpatrick, J. Brown and J. H. Gillard, Identifying Inflamed Carotid Plaques Using *In Vivo* USPIO-Enhanced MR Imaging to Label Plaque Macrophages, *Arterioscler., Thromb., Vasc. Biol.*, 2006, **26**, 1601–1606, DOI: 10.1161/01.ATV.0000222920.59760.df.

28 T. Y. Tang, S. P. S. Howarth, S. R. Miller, M. J. Graves, A. J. Patterson, J.-M. U-King-Im, Z. Y. Li, S. R. Walsh, A. P. Brown, P. J. Kirkpatrick, E. A. Warburton, P. D. Hayes, K. Varty, J. R. Boyle, M. E. Gaunt, A. Zalewski and J. H. Gillard, The ATHEROMA (Atorvastatin Therapy: Effects on Reduction of Macrophage Activity) Study, *J. Am. Coll. Cardiol.*, 2009, **53**, 2039–2050, DOI: 10.1016/j.jacc.2009.03.018.

29 K. Morishige, D. F. Kacher, P. Libby, L. Josephson, P. Ganz, R. Weissleder and M. Aikawa, High-Resolution Magnetic Resonance Imaging Enhanced With Superparamagnetic Nanoparticles Measures Macrophage Burden in Atherosclerosis, *Circulation*, 2010, **122**, 1707–1715, DOI: 10.1161/CIRCULATIONAHA.109.891804.

Open Access Article. Published on 02 4 2024. Downloaded on 2024-08-05 11:52:04.
This article is licensed under a Creative Commons Attribution 3.0 Unported Licence.

30 K. H. Zheng, J. Schoormans, L. C. A. Stiekema, C. Calcagno, I. Cicha, C. Alexiou, G. J. Strijkers, A. J. Nederveen, E. S. G. Stroes and B. F. Coolen, Plaque Permeability Assessed With DCE-MRI Associates With USPIO Uptake in Patients With Peripheral Artery Disease, *JACC Cardiovasc. Imaging*, 2019, **12**, 2081–2083, DOI: 10.1016/j.jcmg.2019.04.014.

31 J. M. S. Chan, P. S. Jin, M. Ng, J. Garnell, C. W. Ying, C. T. Tec and K. Bhakoo, Development of Molecular Magnetic Resonance Imaging Tools for Risk Stratification of Carotid Atherosclerotic Disease Using Dual-Targeted Microparticles of Iron Oxide, Transl, *Stroke Res.*, 2022, **13**, 245–256, DOI: 10.1007/s12975-021-00931-3.

32 S. Bonnet, G. Prévot, S. Mornet, M.-J. Jacobin-Valat, Y. Mousli, A. Hemadou, M. Duttine, A. Trotier, S. Sanchez, M. Duonor-Cérutti, S. Crauste-Manciet and G. Clofent-Sanchez, A Nano-Emulsion Platform Functionalized with a Fully Human scFv-Fc Antibody for Atheroma Targeting: Towards a Theranostic Approach to Atherosclerosis, *Int. J. Mol. Sci.*, 2021, **22**, 5188, DOI: 10.3390/ijms22105188.

33 F. M. E. Segers, A. V. Ruder, M. M. Westra, T. Lammers, S. M. Dadfar, K. Roemhild, T. S. Lam, M. E. Kooi, K. B. J. M. Cleutjens, F. K. Verheyen, G. W. H. Schurink, G. R. Haenen, T. J. C. Van Berkel, I. Bot, B. Halvorsen, J. C. Sluimer and E. A. L. Biessen, Magnetic resonance imaging contrast-enhancement with superparamagnetic iron oxide nanoparticles amplifies macrophage foam cell apoptosis in human and murine atherosclerosis, *Cardiovasc. Res.*, 2023, **118**, 3346–3359, DOI: 10.1093/cvr/cvac032.

34 B. Zinnhardt, M. Wiesmann, L. Honold, C. Barca, M. Schäfers, A. J. Kiliaan and A. H. Jacobs, *In vivo* imaging biomarkers of neuroinflammation in the development and assessment of stroke therapies - towards clinical translation, *Theranostics*, 2018, **8**, 2603–2620, DOI: 10.7150/thno.24128.

35 M. Wiart, C. Tavakoli, V. Hubert, I. Hristovska, C. Dumot, S. Parola, F. Lerouge, F. Chauveau, E. Canet-Soulas, O. Pascual, D. P. Cormode, E. Brun and H. Elleaume, Use of metal-based contrast agents for *in vivo* MR and CT imaging of phagocytic cells in neurological pathologies, *J. Neurosci. Methods*, 2023, **383**, 109729, DOI: 10.1016/j.jneumeth.2022.109729.

36 T. Tourdias, S. Roggerone, M. Filippi, M. Kanagaki, M. Rovaris, D. H. Miller, K. G. Petry, B. Brochet, J.-P. Pruvo, E.-W. Radüe and V. Dousset, Assessment of Disease Activity in Multiple Sclerosis Phenotypes with Combined Gadolinium- and Superparamagnetic Iron Oxide–enhanced MR Imaging, *Radiology*, 2012, **264**, 225–233, DOI: 10.1148/radiol.12111416.

37 A. Saleh, M. Schroeter, A. Ringelstein, H.-P. Hartung, M. Siebler, U. Mödder and S. Jander, Iron Oxide Particle-Enhanced MRI Suggests Variability of Brain Inflammation at Early Stages After Ischemic Stroke, *Stroke*, 2007, **38**, 2733–2737, DOI: 10.1161/STROKEAHA.107.481788.

38 H. L. Walter, M. Walberer, M. A. Rueger, H. Backes, D. Wiedermann, M. Hoehn, B. Neumaier, R. Graf, G. R. Fink and M. Schroeter, *In vivo* analysis of neuroinflammation in the late chronic phase after experimental stroke, *Neuroscience*, 2015, **292**, 71–80, DOI: 10.1016/j.neuroscience.2015.02.024.

39 N. Nighoghossian, M. Wiart and Y. Berthezene, Novel Applications of Magnetic Resonance Imaging to Image Tissue Inflammation after Stroke, *J Neuroimaging*, 2008, **18**, 349–352, DOI: 10.1111/j.1552-6569.2007.00219.x.

40 A. Saleh, D. Wiedermann, M. Schroeter, C. Jonkmanns, S. Jander and M. Hoehn, Central nervous system inflammatory response after cerebral infarction as detected by magnetic resonance imaging, *NMR Biomed.*, 2004, **17**, 163–169, DOI: 10.1002/nbm.881.

41 D. Hasan, N. Chalouhi, P. Jabbour, A. S. Dumont, D. K. Kung, V. A. Magnotta, W. L. Young, T. Hashimoto, H. R. Winn and D. Heistad, Early Change in Ferumoxytol-Enhanced Magnetic Resonance Imaging Signal Suggests Unstable Human Cerebral Aneurysm: A Pilot Study, *Stroke*, 2012, **43**, 3258–3265, DOI: 10.1161/STROKEAHA.112.673400.

42 D. M. Hasan, N. Chalouhi, P. Jabbour, V. A. Magnotta, D. K. Kung and W. L. Young, Imaging aspirin effect on macrophages in the wall of human cerebral aneurysms using ferumoxytol-enhanced MRI: Preliminary results, *J. Neuroradiol.*, 2013, **40**, 187–191, DOI: 10.1016/j.neurad.2012.09.002.

43 D. M. Hasan, M. Amans, T. Tihan, C. Hess, Y. Guo, S. Cha, H. Su, A. J. Martin, M. T. Lawton, E. A. Neuwelt, D. A. Saloner and W. L. Young, Ferumoxytol-Enhanced MRI to Image Inflammation Within Human Brain Arteriovenous Malformations: a Pilot Investigation, Transl, *Stroke Res.*, 2012, **3**, 166–173, DOI: 10.1007/s12975-012-0172-y.

44 A. Nchimi, O. Defawe, D. Brisbois, T. K. Y. Broussaud, J.-O. Defraigne, P. Magotteaux, B. Massart, J.-M. Serfaty, X. Houard, J.-B. Michel and N. Sakalihasan, MR Imaging of Iron Phagocytosis in Intraluminal Thrombi of Abdominal Aortic Aneurysms in Humans, *Radiology*, 2010, **254**, 973–981, DOI: 10.1148/radiol.09090657.

45 S. Khan, F. M. Amin, F. P. Fliedner, C. E. Christensen, D. Tolnai, S. Younis, A. C. R. Olinger, H. Birgens, H. Daldrup-Link, A. Kjær, H. B. W. Larsson, U. Lindberg and M. Ashina, Investigating macrophage-mediated inflammation in migraine using ultrasmall superparamagnetic iron oxide-enhanced 3T magnetic resonance imaging, *Cephalalgia*, 2019, **39**, 1407–1420, DOI: 10.1177/0333102419848122.

46 S. C. Beeman, M. Zhang, L. Gubhaju, T. Wu, J. F. Bertram, D. H. Frakes, B. R. Cherry and K. M. Bennett, Measuring glomerular number and size in perfused kidneys using MRI, *Am. J. Physiol. –Ren. Physiol.*, 2011, **300**, F1454–F1457, DOI: 10.1152/ajprenal.00044.2011.

47 K. M. Bennett, H. Zhou, J. P. Sumner, S. J. Dodd, N. Bouraoud, K. Doi, R. A. Star and A. P. Koretsky, MRI of the basement membrane using charged nanoparticles as

 © 2024 The Author(s). Published by the Royal Society of Chemistry

Open Access Article. Published on 02 4 2024. Downloaded on 2024-08-05 11:52:04.
This article is licensed under a Creative Commons Attribution 3.0 Unported Licence.

contrast agents, *Magn. Reson. Med.*, 2008, **60**, 564–574, DOI: 10.1002/mrm.21684.

48 L. Tillman, T. A. Tabish, N. Kamaly, P. Moss, A. El-briri, C. Thiemermann, M. Z. I. Pranjol and M. M. Yaqoob, Advancements in nanomedicines for the detection and treatment of diabetic kidney disease, *Biomater. Biosyst.*, 2022, **6**, 100047, DOI: 10.1016/j.bbiosy.2022.100047.

49 N. J. Serkova, B. Renner, B. A. Larsen, C. R. Stoldt, K. M. Hasebroock, E. L. Bradshaw-Pierce, V. M. Holers and J. M. Thurman, Renal Inflammation: Targeted Iron Oxide Nanoparticles for Molecular MR Imaging in Mice, *Radiology*, 2010, **255**, 517–526, DOI: 10.1148/radiol.09091134.

50 O. Hauger, N. Grenier, C. Deminère, C. Lasseur, Y. Delmas, P. Merville and C. Combe, USPIO-enhanced MR imaging of macrophage infiltration in native and transplanted kidneys: initial results in humans, *Eur. Radiol.*, 2007, **17**, 2898–2907, DOI: 10.1007/s00330-007-0660-8.

51 Y. Wu, Q. Huang, J. Wang, Y. Dai, M. Xiao, Y. Li, H. Zhang and W. Xiao, The Feasibility of Targeted Magnetic Iron Oxide Nanoagent for Noninvasive IgA Nephropathy Diagnosis, *Front. bioeng. biotechnol.*, 2021, **9**, 755692, DOI: 10.3389/fbioe.2021.755692.

52 Y. Wu, *Application of Macrophage Imaging in Evaluating Disease Activity of Inflammatory Bowel Disease*, 2013, DOI: 10.1594/ECR2013/C-1749.

53 Y. Wu, *MR Tracking SPIO-Labeled Macrophages in Monitoring Inflammatory Bowel Disease (IBD) and Evaluating Disease Activity*, 2012, DOI: 10.1594/ECR2012/C-1224.

54 A. Luciani, S. Dechoux, V. Deveaux, M. Poirier-Quinot, N. Luciani, M. Levy, S. Ballet, S. Manin, C. Péchoux, G. Autret, O. Clément, A. Rahmouni, A. Mallat, C. Wilhelm, S. Lotersztajn and F. Gazeau, Adipose Tissue Macrophages: MR Tracking to Monitor Obesity-associated Inflammation, *Radiology*, 2012, **263**, 786–793, DOI: 10.1148/radiol.12111957.

55 A. De Roos, Science to Practice: Why Follow the Track of Macrophages in Obesity?, *Radiology*, 2012, **263**, 623–625, DOI: 10.1148/radiol.12120418.

56 S. Lefevre, D. Ruimy, F. Jehl, A. Neuville, P. Robert, C. Sordet, M. Ehlinger, J.-L. Dietemann and G. Bierry, Septic Arthritis: Monitoring with USPIO-enhanced Macrophage MR Imaging, *Radiology*, 2011, **258**, 722–728, DOI: 10.1148/radiol.10101272.

57 G. Bierry, F. Jehl, N. Boehm, P. Robert, J.-L. Dietemann and S. Kremer, Macrophage imaging by USPIO-enhanced MR for the differentiation of infectious osteomyelitis and aseptic vertebral inflammation, *Eur. Radiol.*, 2009, **19**, 1604–1611, DOI: 10.1007/s00330-009-1319-4.

58 G. Bierry, F. Jehl, N. Boehm, P. Robert, G. Prévost, J.-L. Dietemann, H. Desal and S. Kremer, Macrophage Activity in Infected Areas of an Experimental Vertebral Osteomyelitis Model: USPIO-enhanced MR Imaging—Feasibility Study, *Radiology*, 2008, **248**, 114–123, DOI: 10.1148/radiol.2481071260.

59 S. A. Schmitz, T. Albrecht and K.-J. Wolf, MR Angiography with Superparamagnetic Iron Oxide: Feasibility Study, *Radiology*, 1999, **213**, 603–607, DOI: 10.1148/radiology.213.2.r99oc24603.

60 K. H. Ahlström, L. O. Johansson, J. B. Rodenburg, A. S. Ragnarsson, P. Åkeson and A. Börseth, Pulmonary MR Angiography with Ultrasmall Superparamagnetic Iron Oxide Particles as a Blood Pool Agent and a Navigator Echo for Respiratory Gating: Pilot Study, *Radiology*, 1999, **211**, 865–869, DOI: 10.1148/radiology.211.3.r99jn10865.

61 H. Ersoy, P. Jacobs, C. K. Kent and M. R. Prince, Blood Pool MR Angiography of Aortic Stent-Graft Endoleak, *Am. J. Roentgenol.*, 2004, **182**, 1181–1186, DOI: 10.2214/ajr.182.5.1821181.

62 M. T. Corwin, G. Fananapazir and A. J. Chaudhari, MR Angiography of Renal Transplant Vasculature with Ferumoxytol, *Acad. Radiol.*, 2016, **23**, 368–373, DOI: 10.1016/j.acra.2015.10.021.

63 M. Wagner, S. Wagner, J. Schnorr, E. Schellenberger, D. Kivelitz, L. Krug, M. Dewey, M. Laule, B. Hamm and M. Taupitz, Coronary MR angiography using citrate-coated very small superparamagnetic iron oxide particles as blood-pool contrast agent: Initial experience in humans, *J. Magn. Reson. Imaging*, 2011, **34**, 816–823, DOI: 10.1002/jmri.22683.

64 H. Sakuma, Coronary CT versus MR Angiography: The Role of MR Angiography, *Radiology*, 2011, **258**, 340–349, DOI: 10.1148/radiol.10100116.

65 Study Record, ClinicalTrials.gov, https://clinicaltrials.gov/study/NCT02954510?cond=NCT02954510&rank=1&limit=10&tab=table, accessed September 14, 2023.

66 M. Wagner, S. Wagner, J. Schnorr, E. Schellenberger, D. Kivelitz, L. Krug, M. Dewey, M. Laule, B. Hamm and M. Taupitz, Coronary MR angiography using citrate-coated very small superparamagnetic iron oxide particles as blood-pool contrast agent: Initial experience in humans, *J. Magn. Reson. Imaging*, 2011, **34**, 816–823, DOI: 10.1002/jmri.22683.

67 C. A. Gharagouzloo, L. Timms, J. Qiao, Z. Fang, J. Nneji, A. Pandya, P. Kulkarni, A. L. Van De Ven, C. Ferris and S. Sridhar, Quantitative vascular neuroimaging of the rat brain using superparamagnetic nanoparticles: New insights on vascular organization and brain function, *Neuroimage*, 2017, **163**, 24–33, DOI: 10.1016/j.neuroimage.2017.09.003.

68 M. Thrippleton, G. Blair, M. Valdes-Hernandez, A. Glatz, S. Semple, F. Doubal, A. Vesey, I. Marshall, D. Newby and J. Wardlaw, MRI Relaxometry for Quantitative Analysis of USPIO Uptake in Cerebral Small Vessel Disease, *Int. J. Mol. Sci.*, 2019, **20**, 776, DOI: 10.3390/ijms20030776.

69 E. A. Neuwelt, B. E. Hamilton, C. G. Varallyay, W. R. Rooney, R. D. Edelman, P. M. Jacobs and S. G. Watnick, Ultrasmall superparamagnetic iron oxides (USPIOs): a future alternative magnetic resonance (MR) contrast agent for patients at risk for nephrogenic systemic fibrosis (NSF)?, *Kidney Int.*, 2009, **75**, 465–474, DOI: 10.1038/ki.2008.496.

70 M. Sigovan, W. Gasper, H. F. Alley, C. D. Owens and D. Saloner, USPIO-enhanced MR Angiography of

Open Access Article. Published on 02 4 2024. Downloaded on 2024-08-05 11:52:04.
This article is licensed under a Creative Commons Attribution 3.0 Unported Licence.

Arteriovenous Fistulas in Patients with Renal Failure, *Radiology*, 2012, **265**, 584–590, DOI: 10.1148/radiol.12112694.

71 P. Zamecnik, B. Israel, J. Feuerstein, J. Nagarajah, M. Gotthardt, J. O. Barentsz and T. Hambrock, Ferumoxtran-10-enhanced 3-T Magnetic Resonance Angiography of Pelvic Arteries: Initial Experience, *Eur. Urol. Focus*, 2022, **8**, 1802–1808, DOI: 10.1016/j.euf.2022.03.001.

72 L. Timms, T. Zhou, Y. Lyu, J. Qiao, V. Mishra, R. M. Lahoud, G. V. Jayaraman, A. S. Allegretti, D. Drew, R. T. Seethamraju, M. Harisinghani and S. Sridhar, Ferumoxytol-enhanced ultrashort TE MRA and quantitative morphometry of the human kidney vasculature, *Abdom. Radiol.*, 2021, **46**, 3288–3300, DOI: 10.1007/s00261-021-02984-2.

73 T.-H. Shin, P. K. Kim, S. Kang, J. Cheong, S. Kim, Y. Lim, W. Shin, J.-Y. Jung, J. D. Lah, B. W. Choi and J. Cheon, High-resolution T_1 MRI via renally clearable dextran nanoparticles with an iron oxide shell, *Nat. Biomed. Eng.*, 2021, **5**, 252–263, DOI: 10.1038/s41551-021-00687-z.

74 C. Li, Clinical Study of Domestic Polysaccharide Superparamagnetic Iron Oxide Nanoparticle Injection for Renal Artery Contrast-enhanced Magnetic Resonance Imaging, clinicaltrials.gov, 2023, https://clinicaltrials.gov/study/NCT05045872, accessed September 14, 2023.

75 S. Buch, Y. Wang, M.-G. Park, P. K. Jella, J. Hu, Y. Chen, K. Shah, Y. Ge and E. M. Haacke, Subvoxel vascular imaging of the midbrain using USPIO-Enhanced MRI, *Neuroimage*, 2020, **220**, 117106, DOI: 10.1016/j.neuroimage.2020.117106.

76 S. Buch, K. Subramanian, P. K. Jella, Y. Chen, Z. Wu, K. Shah, E. Bernitsas, Y. Ge and E. M. Haacke, Revealing vascular abnormalities and measuring small vessel density in multiple sclerosis lesions using USPIO, *NeuroImage Clin.*, 2021, **29**, 102525, DOI: 10.1016/j.nicl.2020.102525.

77 S. Buch, Y. Chen, P. Jella, Y. Ge and E. M. Haacke, Vascular mapping of the human hippocampus using Ferumoxytol-enhanced MRI, *Neuroimage*, 2022, **250**, 118957, DOI: 10.1016/j.neuroimage.2022.118957.

78 Jasmin, G. T. Souza, R. Andrade Louzada, P. H. Rosado-de-Castro, R. Mendez-Otero and A. C. C. Carvalho, Tracking stem cells with superparamagnetic iron oxide nanoparticles: perspectives and considerations, *Int. J. Nanomed.*, 2017, **12**, 779–793, DOI: 10.2147/IJN.S126530.

79 N. Hawrylak, P. Ghosh, J. Broadus, C. Schlueter, W. T. Greenough and P. C. Lauterbur, Nuclear Magnetic Resonance (NMR) Imaging of Iron Oxide-Labeled Neural Transplants, *Exp. Neurol.*, 1993, **121**, 181–192, DOI: 10.1006/exnr.1993.1085.

80 M. Hoehn, E. Küstermann, J. Blunk, D. Wiedermann, T. Trapp, S. Wecker, M. Föcking, H. Arnold, J. Hescheler, B. K. Fleischmann, W. Schwindt and C. Bührle, Monitoring of implanted stem cell migration *in vivo* : A highly resolved *in vivo* magnetic resonance imaging investigation of experimental stroke in rat, *Proc. Natl. Acad. Sci. U. S. A.*, 2002, **99**, 16267–16272, DOI: 10.1073/pnas.242435499.

81 Y. Amsalem, Y. Mardor, M. S. Feinberg, N. Landa, L. Miller, D. Daniels, A. Ocherashvilli, R. Holbova, O. Yosef, I. M. Barbash and J. Leor, Iron-Oxide Labeling and Outcome of Transplanted Mesenchymal Stem Cells in the Infarcted Myocardium, *Circulation*, 2007, **116**, 38–45, DOI: 10.1161/CIRCULATIONAHA.106.680231.

82 C. Chapon, J. S. Jackson, E. O. Aboagye, A. H. Herlihy, W. A. Jones and K. K. Bhakoo, An *In Vivo* Multimodal Imaging Study Using MRI and PET of Stem Cell Transplantation after Myocardial Infarction in Rats, Mol, *Imaging Biol.*, 2009, **11**, 31–38, DOI: 10.1007/s11307-008-0174-z.

83 N. K. Lee, H. S. Kim, D. Yoo, J. W. Hwang, S. J. Choi, W. Oh, J. W. Chang and D. L. Na, Magnetic Resonance Imaging of Ferumoxytol-Labeled Human Mesenchymal Stem Cells in the Mouse Brain, *Stem Cell Rev. Rep.*, 2017, **13**, 127–138, DOI: 10.1007/s12015-016-9694-0.

84 A. M. Hamilton, W.-Y. Cheung, A. Gómez-Aristizábal, A. Sharma, S. Nakamura, A. Chaboureau, S. Bhatt, R. Rabani, M. Kapoor, P. J. Foster and S. Viswanathan, Iron nanoparticle-labeled murine mesenchymal stromal cells in an osteoarthritic model persists and suggests anti-inflammatory mechanism of action, *PLoS One*, 2019, **14**, e0214107, DOI: 10.1371/journal.pone.0214107.

85 J. Yan, T. Liu, Y. Li, J. Zhang, B. Shi, F. Zhang, X. Hou, X. Zhang, W. Cui, J. Li, H. Yao, X. Li, Y. Gao and J. Jiang, Effects of magnetically targeted iron oxide@polydopamine-labeled human umbilical cord mesenchymal stem cells in cerebral infarction in mice, *Aging*, 2023, **15**(4), 1130–1142, DOI: 10.18632/aging.204540.

86 L. Duan, J. Zuo, F. Zhang, B. Li, Z. Xu, H. Zhang, B. Yang, W. Song and J. Jiang, Magnetic Targeting of HU-MSCs in the Treatment of Glucocorticoid-Associated Osteonecrosis of the Femoral Head Through Akt/Bcl2/Bad/Caspase-3 Pathway, *Int. J. Nanomed.*, 2020, **15**, 3605–3620, DOI: 10.2147/IJN.S244453.

87 X. Li, Z. Wei, B. Li, J. Li, H. Lv, L. Wu, H. Zhang, B. Yang, M. Zhu and J. Jiang, *In vivo* migration of Fe_3O_4 @polydopamine nanoparticle-labeled mesenchymal stem cells to burn injury sites and their therapeutic effects in a rat model, *Biomater. Sci.*, 2019, **7**, 2861–2872, DOI: 10.1039/C9BM00242A.

88 N. Di Maggio, E. Martella, S. Meikle, M. Columbaro, E. Lucarelli, M. Santin and A. Banfi, Rapid and efficient magnetization of mesenchymal stem cells by dendrimer-functionalized magnetic nanoparticles, *Nanomed*, 2016, **11**, 1519–1534, DOI: 10.2217/nnm-2016-0085.

89 Q. Wang, B. Chen, M. Cao, J. Sun, H. Wu, P. Zhao, J. Xing, Y. Yang, X. Zhang, M. Ji and N. Gu, Response of MAPK pathway to iron oxide nanoparticles in vitro treatment promotes osteogenic differentiation of hBMSCs, *Biomaterials*, 2016, **86**, 11–20, DOI: 10.1016/j.biomaterials.2016.02.004.

90 P. Jiang, Y. Zhang, C. Zhu, W. Zhang, Z. Mao and C. Gao, Fe_3O_4/BSA particles induce osteogenic differentiation of

 © 2024 The Author(s). Published by the Royal Society of Chemistry

Open Access Article. Published on 02 4 2024. Downloaded on 2024-08-05 11:52:04.
This article is licensed under a Creative Commons Attribution 3.0 Unported Licence.

mesenchymal stem cells under static magnetic field, *Acta Biomater.*, 2016, **46**, 141–150, DOI: 10.1016/j.actbio.2016.09.020.

91 X. Li, Z. Wei, H. Lv, L. Wu, Y. Cui, H. Yao, J. Li, H. Zhang, B. Yang and J. Jiang, Iron oxide nanoparticles promote the migration of mesenchymal stem cells to injury sites, *Int. J. Nanomed.*, 2019, **14**, 573–589, DOI: 10.2147/IJN.S184920.

92 M. A. Kolecka, S. Arnhold, M. Schmidt, C. Reich, M. Kramer, K. Failing and K. Von Pückler, Behaviour of adipose-derived canine mesenchymal stem cells after superparamagnetic iron oxide nanoparticles labelling for magnetic resonance imaging, *BMC Vet. Res.*, 2016, **13**, 62, DOI: 10.1186/s12917-017-0980-0.

93 C. Tang, P. J. Russell, R. Martiniello-Wilks, J. E. J. Rasko and A. Khatri, Concise review: Nanoparticles and cellular carriers-allies in cancer imaging and cellular gene therapy?, *Stem Cells*, 2010, **28**, 1686–1702, DOI: 10.1002/stem.473.

94 F.-T. Hsu, Z.-H. Wei, Y. C.-Y. Hsuan, W. Lin, Y.-C. Su, C.-H. Liao and C.-L. Hsieh, MRI tracking of polyethylene glycol-coated superparamagnetic iron oxide-labelled placenta-derived mesenchymal stem cells toward glioblastoma stem-like cells in a mouse model, *Artif. Cells, Nanomed., Biotechnol.*, 2018, **46**, 448–459, DOI: 10.1080/21691401.2018.1499661.

95 J. Hunger, K. Schregel, M. Fischer, D. A. Agardy, V. Sturm, K. Karimian-Jazi, T. Bunse, S. Heiland, W. Wick, M. Bendszus, M. Platten and M. O. Breckwoldt, Non-invasive tracking of T-cell recruitment to the tumor microenvironment in a murine glioma model by high field cellular MRI, in *WFNOS 2022 Abstr. Book, the Korean Brain Tumor Society; the Korean Society for Neuro-Oncology; the Korean Society for Pediatric Neuro-Oncology*, Korea, 2022, p. S329. DOI: 10.14791/btrt.2022.10.F-1268.

96 M. Torabi, S. L. Aquino and M. G. Harisinghani, Current concepts in lymph node imaging, *J. Nucl. Med. Off. Publ. Soc. Nucl. Med.*, 2004, **45**, 1509–1518.

97 M. Saksena, M. Harisinghani, P. Hahn, J. Kim, A. Saokar, B. King and R. Weissleder, Comparison of Lymphotropic Nanoparticle-Enhanced MRI Sequences in Patients with Various Primary Cancers, *Am. J. Roentgenol.*, 2006, **187**, W582–W588, DOI: 10.2214/AJR.05.0873.

98 Y. Anzai and M. R. Prince, Iron oxide-enhanced MR lymphography: The evaluation of cervical lymph node metastases in head and neck cancer, *J. Magn. Reson. Imaging*, 1997, **7**, 75–81, DOI: 10.1002/jmri.1880070111.

99 C. Stets, S. Brandt, F. Wallis, J. Buchmann, F. J. Gilbert and S. H. Heywang-Köbrunner, Axillary lymph node metastases: A statistical analysis of various parameters in MRI with USPIO: Axillary Lymph Node Metastases, *J. Magn. Reson. Imaging*, 2002, **16**, 60–68, DOI: 10.1002/jmri.10134.

100 B. C. Nguyen, W. Stanford, B. H. Thompson, N. P. Rossi, K. H. Kernstine, J. A. Kern, R. A. Robinson, J. K. Amorosa, J. F. Mammone and E. K. Outwater, Multicenter clinical trial of ultrasmall superparamagnetic iron oxide in the evaluation of mediastinal lymph nodes in patients with primary lung carcinoma, *J. Magn. Reson. Imaging*, 1999, **10**, 468–473, DOI: 10.1002/(SICI)1522-2586(199909)10:3<468::AID-JMRI31>3.0.CO;2-I.

101 B. B. Pultrum, Detection of lymph node metastases with ultrasmall superparamagnetic iron oxide (USPIO)-enhanced magnetic resonance imaging in oesophageal cancer: a feasibility study, *Cancer Imag.*, 2009, **9**, 19–28, DOI: 10.1102/1470-7330.2009.0004.

102 T. Tokuhara, N. Tanigawa, M. Matsuki, E. Nomura, H. Mabuchi, S.-W. Lee, Y. Tatsumi, H. Nishimura, R. Yoshinaka, Y. Kurisu and I. Narabayashi, Evaluation of lymph node metastases in gastric cancer using magnetic resonance imaging with ultrasmall superparamagnetic iron oxide (USPIO): diagnostic performance in post-contrast images using new diagnostic criteria, *Gastric Cancer*, 2008, **11**, 194–200, DOI: 10.1007/s10120-008-0480-9.

103 M. J. Lahaye, S. M. E. Engelen, A. G. H. Kessels, A. P. De Bruïne, M. F. Von Meyenfeldt, J. M. A. Van Engelshoven, C. J. H. Van De Velde, G. L. Beets and R. G. H. Beets-Tan, USPIO-enhanced MR Imaging for Nodal Staging in Patients with Primary Rectal Cancer: Predictive Criteria, *Radiology*, 2008, **246**, 804–811, DOI: 10.1148/radiol.2463070221.

104 P. Narayanan, T. Iyngkaran, S. A. Sohaib, R. H. Reznek and A. G. Rockall, Pearls and Pitfalls of MR Lymphography in Gynecologic Malignancy, *Radiographics*, 2009, **29**, 1057–1069, DOI: 10.1148/rg.294085231.

105 H. C. Thoeny, M. Triantafyllou, F. D. Birkhaeuser, J. M. Froehlich, D. W. Tshering, T. Binser, A. Fleischmann, P. Vermathen and U. E. Studer, Combined Ultrasmall Superparamagnetic Particles of Iron Oxide–Enhanced and Diffusion-Weighted Magnetic Resonance Imaging Reliably Detect Pelvic Lymph Node Metastases in Normal-Sized Nodes of Bladder and Prostate Cancer Patients, *Eur. Urol.*, 2009, **55**, 761–769, DOI: 10.1016/j.eururo.2008.12.034.

106 O. A. Debats, A. S. Fortuin, H. J. M. Meijer, T. Hambrock, G. J. S. Litjens, J. O. Barentsz and H. J. Huisman, Intranodal signal suppression in pelvic MR lymphography of prostate cancer patients: a quantitative comparison of ferumoxtran-10 and ferumoxytol, *PeerJ*, 2016, **4**, e2471, DOI: 10.7717/peerj.2471.

107 B. Turkbey, H. K. Agarwal, J. Shih, M. Bernardo, Y. L. McKinney, D. Daar, G. L. Griffiths, S. Sankineni, L. Johnson, K. B. Grant, J. Weaver, S. Rais-Bahrami, M. Harisinghani, P. Jacobs, W. Dahut, M. J. Merino, P. A. Pinto and P. L. Choyke, A Phase I Dosing Study of Ferumoxytol for MR Lymphography at 3T in Patients With Prostate Cancer, *Am. J. Roentgenol.*, 2015, **205**, 64–69, DOI: 10.2214/AJR.14.13009.

108 S. Woo, C. H. Suh, S. Y. Kim, J. Y. Cho and S. H. Kim, The Diagnostic Performance of MRI for Detection of Lymph Node Metastasis in Bladder and Prostate Cancer: An Updated Systematic Review and Diagnostic Meta-Analysis, *Am. J. Roentgenol.*, 2018, **210**, W95–W109, DOI: 10.2214/AJR.17.18481.

Open Access Article. Published on 02 4 2024. Downloaded on 2024-08-05 11:52:04.
This article is licensed under a Creative Commons Attribution 3.0 Unported Licence.

109 M. G. M. Schilham, P. Zamecnik, B. M. Privé, B. Israël, M. Rijpkema, T. Scheenen, J. O. Barentsz, J. Nagarajah and M. Gotthardt, Head-to-Head Comparison of 68 Ga-Prostate-Specific Membrane Antigen PET/CT and Ferumoxtran-10–Enhanced MRI for the Diagnosis of Lymph Node Metastases in Prostate Cancer Patients, *J. Nucl. Med.*, 2021, **62**, 1258–1263, DOI: 10.2967/jnumed.120.258541.

110 Saving Patients' Lives Medical B.V., A Confirmatory, Prospective, Open-label, Single-arm, Reader-blinded Multi-centre Phase 3 Study to Assess the Diagnostic Accuracy of Ferumoxtran-10-enhanced Magnetic Resonance Imaging (MRI) and Unenhanced MRI in Reference to Histopathology in Newly-diagnosed Prostate Cancer (PCA) Patients, Scheduled for Radical Prostatectomy (RP) With Extended Pelvic Lymph Node Dissection (ePLND), clinicaltrials.gov, 2023. https://clinicaltrials.gov/study/NCT04261777, accessed September 12, 2023.

111 R. C. H. Stijns, B. W. J. Philips, I. D. Nagtegaal, F. Polat, J. H. W. de Wilt, C. A. P. Wauters, P. Zamecnik, J. J. Fütterer and T. W. J. Scheenen, USPIO-enhanced MRI of lymph nodes in rectal cancer: A node-to-node comparison with histopathology, *Eur. J. Radiol.*, 2021, **138**, 109636, DOI: 10.1016/j.ejrad.2021.109636.

112 M. D. Anderson Cancer Center, Magnetic Particle-ICG Lymph Node Mapping in Colorectal Cancer, clinicaltrials.gov, 2023. https://clinicaltrials.gov/study/NCT05092750, accessed September 12, 2023.

113 D. A. J. J. Driessen, P. Zámecnik, T. Dijkema, S. A. H. Pegge, A. C. H. Van Engen-van Grunsven, R. P. Takes, J. H. A. M. Kaanders and T. W. J. Scheenen, High-Accuracy Nodal Staging of Head and Neck Cancer With USPIO-Enhanced MRI: A New Reading Algorithm Based on Node-to-Node Matched Histopathology, *Invest. Radiol.*, 2022, **57**, 810–818, DOI: 10.1097/RLI.0000000000000902.

114 B. Turkbey, M. Czarniecki, J. H. Shih, S. A. Harmon, P. K. Agarwal, A. B. Apolo, D. E. Citrin, J. L. Gulley, M. Harisinghani, R. A. Madan, A. R. Metwalli, E. Paquette, P. A. Pinto, S. Rais-Bahrami, L. S. Rowe, B. J. Wood, P. M. Jacobs, L. Lindenberg, W. Dahut and P. L. Choyke, Ferumoxytol-Enhanced MR Lymphography for Detection of Metastatic Lymph Nodes in Genitourinary Malignancies: A Prospective Study, *Am. J. Roentgenol.*, 2020, **214**, 105–113, DOI: 10.2214/AJR.19.21264.

115 A. O'Shea, A. Parakh, R. M. Lahoud, S. Hedgire and M. G. Harisinghani, The Evolution of Iron Oxide Nanoparticles as MRI Contrast Agents, *MRS Adv.*, 2020, **5**, 2157–2168, DOI: 10.1557/adv.2020.311.

116 B. W. J. Philips, R. C. H. Stijns, S. H. G. Rietsch, S. Brunheim, J. O. Barentsz, A. S. Fortuin, H. H. Quick, S. Orzada, M. C. Maas and T. W. J. Scheenen, USPIO-enhanced MRI of pelvic lymph nodes at 7-T: preliminary experience, *Eur. Radiol.*, 2019, **29**, 6529–6538, DOI: 10.1007/s00330-019-06277-7.

117 X.-Q. He and L.-N. Wei, Diagnostic value of lymph node metastasis by diffusion-weighted magnetic resonance imaging in cervical cancer, *J. Cancer Res. Ther.*, 2016, **12**, 77, DOI: 10.4103/0973-1482.148726.

118 K. Motomura, T. Izumi, S. Tateishi, Y. Tamaki, Y. Ito, T. Horinouchi and K. Nakanishi, Superparamagnetic iron oxide-enhanced MRI at 3 T for accurate axillary staging in breast cancer, *Br. J. Surg.*, 2015, **103**, 60–69, DOI: 10.1002/bjs.10040.

119 K. Motomura, Y. Tabuchi, Y. Enomoto, T. Nishida, T. Nakaoka, D. Mori and M. Kouda, Accurate axillary staging by superparamagnetic iron oxide-enhanced MRI at 1.5 T with fat-suppression sequence as an alternative to sentinel node biopsy in breast cancer, *Br. J. Surg.*, 2021, **108**, e359–e360, DOI: 10.1093/bjs/znab277.

120 N. Mirzaei, D. Katsarelias, P. Zaar, O. Jalnefjord, I. Johansson, H. Leonhardt, F. Wärnberg and R. Olofsson Bagge, Sentinel lymph node localization and staging with a low-dose of superparamagnetic iron oxide (SPIO) enhanced MRI and magnetometer in patients with cutaneous melanoma of the extremity - The MAGMEN feasibility study, *Eur. J. Surg. Oncol.*, 2022, **48**, 326–332, DOI: 10.1016/j.ejso.2021.12.467.

121 A. Jazrawi, E. Pantiora, S. Abdsaleh, D. V. Bacovia, S. Eriksson, H. Leonhardt, F. Wärnberg and A. Karakatsanis, Magnetic-Guided Axillary UltraSound (MagUS) Sentinel Lymph Node Biopsy and Mapping in Patients with Early Breast Cancer. A Phase 2, Single-Arm Prospective Clinical Trial, *Cancers*, 2021, **13**, 4285, DOI: 10.3390/cancers13174285.

122 A. Jazrawi, E. Pantiora, S. Abdsaleh, D. V. Bacovia, S. Eriksson, H. Leonhardt, F. Wärnberg and A. Karakatsanis, Magnetic-Guided Axillary UltraSound (MagUS) Sentinel Lymph Node Biopsy and Mapping in Patients with Early Breast Cancer. A Phase 2, Single-Arm Prospective Clinical Trial, *Cancers*, 2021, **13**, 4285, DOI: 10.3390/cancers13174285.

123 Radboud University Medical Center, Validation of USPIO-enhanced MRI for Detection of Lymph Node Metastases in Head and Neck Carcinoma: A Pilot Study, clinicaltrials.gov, 2022. https://clinicaltrials.gov/study/NCT03817307, accessed September 12, 2023.

124 D. Katsarelias, Sentinel Node Localisation and Staging With Superparamagnetic Iron Oxide-enhanced MRI and Magtrace®/Sentimag® in Patients With Malignant Melanoma of the Extremities. The MAGMEN Feasibility Study, clinicaltrials.gov, 2020. https://clinicaltrials.gov/study/NCT03898687, accessed September 12, 2023.

125 S. Tong, H. Zhu and G. Bao, Magnetic iron oxide nanoparticles for disease detection and therapy, *Mater. Today*, 2019, **31**, 86–99, DOI: 10.1016/j.mattod.2019.06.003.

126 P. Carmeliet and R. K. Jain, Angiogenesis in cancer and other diseases, *Nature*, 2000, **407**, 249–257, DOI: 10.1038/35025220.

127 X. Montet, K. Montet-Abou, F. Reynolds, R. Weissleder and L. Josephson, Nanoparticle Imaging of Integrins on Tumor Cells, *Neoplasia*, 2006, **8**, 214–222, DOI: 10.1593/neo.05769.

 © 2024 The Author(s). Published by the Royal Society of Chemistry

Open Access Article. Published on 02 4 2024. Downloaded on 2024-08-05 11:52:04.
This article is licensed under a Creative Commons Attribution 3.0 Unported Licence.

128 C. W. Kessinger, O. Togao, C. Khemtong, G. Huang, M. Takahashi and J. Gao, Investigation of *In Vivo* Targeting Kinetics of α_v β_3 -Specific Superparamagnetic Nanoprobes by Time-Resolved MRI, *Theranostics*, 2011, **1**, 263–273, DOI: 10.7150/thno/v01p0263.

129 F. Danhier, To exploit the tumor microenvironment: Since the EPR effect fails in the clinic, what is the future of nanomedicine?, *J. Controlled Release*, 2016, **244**, 108–121, DOI: 10.1016/j.jconrel.2016.11.015.

130 J. Wu, The Enhanced Permeability and Retention (EPR) Effect: The Significance of the Concept and Methods to Enhance Its Application, *J. Pers. Med.*, 2021, **11**, 771, DOI: 10.3390/jpm11080771.

131 L. Wang, J. Huang, H. Chen, H. Wu, Y. Xu, Y. Li, H. Yi, Y. A. Wang, L. Yang and H. Mao, Exerting Enhanced Permeability and Retention Effect Driven Delivery by Ultrafine Iron Oxide Nanoparticles with T_1–T_2 Switchable Magnetic Resonance Imaging Contrast, *ACS Nano*, 2017, **11**, 4582–4592, DOI: 10.1021/acsnano.7b00038.

132 L. Santoro, L. Grazioli, A. Filippone, E. Grassedonio, G. Belli and S. Colagrande, Resovist enhanced MR imaging of the liver: Does quantitative assessment help in focal lesion classification and characterization?, *J. Magn. Reson. Imaging*, 2009, **30**, 1012–1020, DOI: 10.1002/jmri.21937.

133 K. Takeshita, I. Nagashima, S. Frui, K. Takada, T. Yamauchi, A. Harasawa, H. Oba, H. Kohtake, H. Tanaka and S. Suzuki, Effect of Superparamagnetic Iron Oxide-Enhanced MRI of the Liver With Hepatocellular Carcinoma and Hyperplastic Nodule, *J. Comput. Assist. Tomogr.*, 2002, **26**, 451–455, DOI: 10.1097/00004728-200205000-00024.

134 F. Chen, J. Ward and P. J. Robinson, MR imaging of the liver and spleen: a comparison of the effects on signal intensity of two superparamagnetic iron oxide agents, *Magn. Reson. Imaging*, 1999, **17**, 549–556, DOI: 10.1016/S0730-725X(98)00193-3.

135 Y. L. Thian, A. M. Riddell and D.-M. Koh, Liver-specific agents for contrast-enhanced MRI: role in oncological imaging, *Cancer Imag.*, 2013, **13**, 567–579, DOI: 10.1102/1470-7330.2013.0050.

136 J. T. Ferrucci and D. D. Stark, Iron oxide-enhanced MR imaging of the liver and spleen: review of the first 5 years, *Am. J. Roentgenol.*, 1990, **155**, 943–950, DOI: 10.2214/ajr.155.5.2120963.

137 B. E. Hamilton, G. M. Nesbit, E. Dosa, S. Gahramanov, B. Rooney, E. G. Nesbit, J. Raines and E. A. Neuwelt, Comparative Analysis of Ferumoxytol and Gadoteridol Enhancement Using T_1- and T_2-Weighted MRI in Neuroimaging, *Am. J. Roentgenol.*, 2011, **197**, 981–988, DOI: 10.2214/AJR.10.5992.

138 S. Gahramanov, L. L. Muldoon, C. G. Varallyay, X. Li, D. F. Kraemer, R. Fu, B. E. Hamilton, W. D. Rooney and E. A. Neuwelt, Pseudoprogression of Glioblastoma after Chemo- and Radiation Therapy: Diagnosis by Using Dynamic Susceptibility-weighted Contrast-enhanced Perfusion MR Imaging with Ferumoxytol versus Gadoteridol and Correlation with Survival, *Radiology*, 2013, **266**, 842–852, DOI: 10.1148/radiol.12111472.

139 R. J. McDonald, J. S. McDonald, D. F. Kallmes, M. E. Jentoft, D. L. Murray, K. R. Thielen, E. E. Williamson and L. J. Eckel, Intracranial Gadolinium Deposition after Contrast-enhanced MR Imaging, *Radiology*, 2015, **275**, 772–782, DOI: 10.1148/radiol.15150025.

140 M. Iv, P. Samghabadi, S. Holdsworth, A. Gentles, P. Rezaii, G. Harsh, G. Li, R. Thomas, M. Moseley, H. E. Daldrup-Link, H. Vogel, M. Wintermark, S. Cheshier and K. W. Yeom, Quantification of Macrophages in High-Grade Gliomas by Using Ferumoxytol-enhanced MRI: A Pilot Study, *Radiology*, 2019, **290**, 198–206, DOI: 10.1148/radiol.2018181204.

141 F. Ghorbani, R. Irajirad, F. Emami, F. Vaziri Nezamdoust and A. Montazerabadi, Specified iron oxide nanoparticles by PSMA-11 as a promising nanomolecular imaging probe for early detection of prostate cancer, *Appl. Nanosci.*, 2022, **12**, 2291–2304, DOI: 10.1007/s13204-022-02507-5.

142 M. Eivazi, P. M. Khaniabadi, S. H. Hejazi and D. Shahbazi-Gahrouei, Porphyrin–iron oxide nanoparticle functionalized with trastuzumab (ION–PP–TZ) potential MR imaging probe for breast cancer cells, *Appl. Phys. A*, 2022, **128**, 509, DOI: 10.1007/s00339-022-05558-1.

143 C.-W. Yang, K. Liu, C.-Y. Yao, B. Li, A. Juhong, Z. Qiu and X. Huang, Indocyanine Green-Conjugated Superparamagnetic Iron Oxide Nanoworm for Multimodality Breast Cancer Imaging, *ACS Appl. Nano Mater.*, 2022, **5**, 18912–18920, DOI: 10.1021/acsanm.2c04687.

144 Z. Wu, S. Stangl, A. Hernandez-Schnelzer, F. Wang, M. Hasanzadeh Kafshgari, A. Bashiri Dezfouli and G. Multhoff, Functionalized Hybrid Iron Oxide–Gold Nanoparticles Targeting Membrane Hsp70 Radiosensitize Triple-Negative Breast Cancer Cells by ROS-Mediated Apoptosis, *Cancers*, 2023, **15**, 1167, DOI: 10.3390/cancers15041167.

145 C. Chiang, Y. Hsu, W. Hsieh, T. Liao, C. Chen, Y. Chen, P. Liang and S. Wang, IOP Injection, A Novel Superparamagnetic Iron Oxide Particle MRI Contrast Agent for the Detection of Hepatocellular Carcinoma: A Phase II Clinical Trial, *J. Magn. Reson. Imaging*, 2023, **58**, 1177–1188, DOI: 10.1002/jmri.28645.

146 Y. Hama and E. Tate, SPIO-enhanced 0.35T MRI-guided radiotherapy for liver malignancies: usefulness in tumor visualization, *Br. J. Radiol.*, 2022, **95**, 20211131, DOI: 10.1259/bjr.20211131.

147 N. Meher, H. F. VanBrocklin, D. M. Wilson and R. R. Flavell, PSMA-Targeted Nanotheranostics for Imaging and Radiotherapy of Prostate Cancer, *Pharmaceuticals*, 2023, **16**, 315, DOI: 10.3390/ph16020315.

148 T. Nayerpour Dizaj, D. Jafari-Gharabaghlou, M. Farhoudi Sefidan Jadid, R. Jahanban, M. Rahimi, M. Farajollahi, M. Mohsenzadegan and N. Zarghami, Fabrication of Antibody Conjugated Super Magnetic Oxide Nanoparticles for Early Detection of Prostate Cancer, *Asian Pac. J. Cancer*

Open Access Article. Published on 02 4 2024. Downloaded on 2024-08-05 11:52:04.
This article is licensed under a Creative Commons Attribution 3.0 Unported Licence.

Prev., 2023, **24**, 2089–2097, DOI: 10.31557/APJCP.2023.24.6.2089.

149 W. Zhou, J. Huang, Q. Xiao, S. Hu, S. Li, J. Zheng, Z. Du, J. Peng and H. Chen, Glu-Urea-Lys Scaffold Functionalized Superparamagnetic Iron Oxide Nanoparticles Targeting PSMA for *In Vivo* Molecular MRI of Prostate Cancer, *Pharmaceutics*, 2022, **14**, 2051, DOI: 10.3390/pharmaceutics14102051.

150 D. T. Martin, J. S. Lee, Q. Liu, G. Galiana, P. C. Sprenkle, P. A. Humphrey, D. P. Petrylak, J. C. Weinreb, P. G. Schulam, R. M. Weiss and T. M. Fahmy, Targeting prostate cancer with Clostridium perfringens enterotoxin functionalized nanoparticles co-encapsulating imaging cargo enhances magnetic resonance imaging specificity, *Nanomed.: Nanotechnol. Biol. Med.*, 2022, **40**, 102477, DOI: 10.1016/j.nano.2021.102477.

151 M. Zhang, K. Kandasamy, Y. Perera, D. Inglese and E. Smith-Nguyen, Abstract 3586: *In vivo* targeted detection and imaging of ovarian cancer by SPMR and MRI using anti-folate receptor functionalized iron oxide nanoparticles, *Cancer Res.*, 2023, **83**, 3586, DOI: 10.1158/1538-7445.AM2023-3586.

152 A. Kimura, S. Utsumi, A. Shimokawa, R. Nishimori, R. Hosoi, N. J. Stewart, H. Imai and H. Fujiwara, Targeted Imaging of Lung Cancer with Hyperpolarized 129Xe MRI Using Surface-Modified Iron Oxide Nanoparticles as Molecular Contrast Agents, *Cancers*, 2022, **14**, 6070, DOI: 10.3390/cancers14246070.

153 L. Yang, M. J. Afshari, J. Ge, D. Kou, L. Chen, D. Zhou, C. Li, S. Wu, L. Zhang, J. Zeng, J. Zhong, R. H. Stauber and M. Gao, Functionalized Ultrasmall Iron Oxide Nanoparticles for T_1-Weighted Magnetic Resonance Imaging of Tumor Hypoxia, *Molecules*, 2022, **27**, 6929, DOI: 10.3390/molecules27206929.

154 Radboud University Medical Center, Unravelling the Invisible Infiltrating Component of Glioblastoma Using MRI and a Strong Iron-like Bloodpool Contrast Medium?, clinicaltrials.gov, 2022, https://clinicaltrials.gov/study/NCT05656300, accessed September 12, 2023.

155 A. Kirichenko, Adaptive Stereotactic Radiotherapy With Superparamagnetic Iron Oxide Nanoparticles (SPION) Cellular Magnetic Resonance Imaging on MR-Linac (MR-L-SPION) for Primary and Metastatic Hepatic Malignancies With Assessment of Treatment Response, clinicaltrials.gov, 2023, https://clinicaltrials.gov/study/NCT04682847, accessed September 12, 2023.

156 J. Maranchie, Virtual Histology of the Bladder Wall for Bladder Cancer Staging; A Novel Intravesical Contrast-Enhanced MRI for Bladder Cancer Staging, clinicaltrials.gov, 2022, https://clinicaltrials.gov/study/NCT04369560, accessed September 12, 2023.

157 Y. Li, M. Xie, J. B. Jones, Z. Zhang, Z. Wang, T. Dang, X. Wang, M. Lipowska and H. Mao, Targeted Delivery of DNA Topoisomerase Inhibitor SN38 to Intracranial Tumors of Glioblastoma Using Sub-5 Ultrafine Iron Oxide Nanoparticles, *Adv. Healthcare Mater.*, 2022, **11**, 2102816, DOI: 10.1002/adhm.202102816.

158 H. Chen and J. Wen, Iron oxide nanoparticles loaded with paclitaxel inhibits glioblastoma by enhancing autophagy-dependent ferroptosis pathway, *Eur. J. Pharmacol.*, 2022, **921**, 174860, DOI: 10.1016/j.ejphar.2022.174860.

159 Z. Wang, Y. Wang, H. Li, Y. Lan, Z. Zeng, J. Yao, M. Li and H. Xia, Fabrication of Etoposide-loaded superparamagnetic iron oxide nanoparticles (SPIONs) induced apoptosis in glioma cancer cells, *Process Biochem.*, 2023, **128**, 126–136, DOI: 10.1016/j.procbio.2023.02.026.

160 Z. Nie, Y. Vahdani, W. C. Cho, S. H. Bloukh, Z. Edis, S. Haghighat, M. Falahati, R. Kheradmandi, L. A. Jaragh-Alhadad and M. Sharifi, 5-Fluorouracil-containing inorganic iron oxide/platinum nanozymes with dual drug delivery and enzyme-like activity for the treatment of breast cancer, *Arabian J. Chem.*, 2022, **15**, 103966, DOI: 10.1016/j.arabjc.2022.103966.

161 E. P. Hernandes, D. Lazarin-Bidóia, R. D. Bini, C. V. Nakamura, L. F. Cótica and S. De Oliveira Silva Lautenschlager, Doxorubicin-Loaded Iron Oxide Nanoparticles Induce Oxidative Stress and Cell Cycle Arrest in Breast Cancer Cells, *Antioxidants*, 2023, **12**, 237, DOI: 10.3390/antiox12020237.

162 B. Foroughi-Nia, A. Aghanejad, J. Kadkhoda, J. Barar, H. Nosrati and S. Davaran, AS1411 conjugated magnetic-based poly *N* -isopropyl acrylamide nanoparticles for delivery of erlotinib to prostate cancer cells, *Appl. Organomet. Chem.*, 2022, **36**, e6691, DOI: 10.1002/aoc.6691.

163 K.-S. Kim, B. Choi, H. Choi, M. J. Ko, D.-H. Kim and D.-H. Kim, Enhanced natural killer cell anti-tumor activity with nanoparticles mediated ferroptosis and potential therapeutic application in prostate cancer, *J. Nanobiotechnol.*, 2022, **20**, 428, DOI: 10.1186/s12951-022-01635-y.

164 S. Mohaghegh, A. Tarighatnia, Y. Omidi, J. Barar, A. Aghanejad and K. Adibkia, Multifunctional magnetic nanoparticles for MRI-guided co-delivery of erlotinib and L-asparaginase to ovarian cancer, *J. Microencapsulation*, 2022, **39**, 394–408, DOI: 10.1080/02652048.2022.2094487.

165 F. Ashoori, B. Hajipour-Verdom, M. Satari and P. Abdolmaleki, Polyethylenimine-based iron oxide nanoparticles enhance cisplatin toxicity in ovarian cancer cells in the presence of a static magnetic field, *Front. Oncol.*, 2023, **13**, 1217800, DOI: 10.3389/fonc.2023.1217800.

166 M. Ramezani Farani, M. Azarian, H. Heydari Sheikh Hossein, Z. Abdolvahabi, Z. Mohammadi Abgarmi, A. Moradi, S. M. Mousavi, M. Ashrafizadeh, P. Makvandi, M. R. Saeb and N. Rabiee, Folic Acid-Adorned Curcumin-Loaded Iron Oxide Nanoparticles for Cervical Cancer, *ACS Appl. Bio Mater.*, 2022, **5**, 1305–1318, DOI: 10.1021/acsabm.1c01311.

167 F. Serio, N. Silvestri, S. Kumar Avugadda, G. E. P. Nucci, S. Nitti, V. Onesto, F. Catalano, E. D'Amone, G. Gigli, L. L. Del Mercato and T. Pellegrino, Co-loading of doxorubicin and iron oxide nanocubes in polycaprolactone fibers for combining Magneto-Thermal and chemotherapeutic effects on cancer cells, *J. Colloid*

 © 2024 The Author(s). Published by the Royal Society of Chemistry

Open Access Article. Published on 02 4 2024. Downloaded on 2024-08-05 11:52:04.
This article is licensed under a Creative Commons Attribution 3.0 Unported Licence.

Interface Sci., 2022, **607**, 34–44, DOI: 10.1016/j.jcis.2021.08.153.

168 M. Darroudi, S. E. Nazari, F. Asgharzadeh, N. Khalili-Tanha, G. Khalili-Tanha, T. Dehghani, M. Karimzadeh, M. Maftooh, G. A. Fern, A. Avan, M. Rezayi and M. Khazaei, Fabrication and application of cisplatin-loaded mesoporous magnetic nanobiocomposite: a novel approach to smart cervical cancer chemotherapy, *Cancer Nanotechnol.*, 2022, **13**, 36, DOI: 10.1186/s12645-022-00141-y.

169 Y.-C. Chin, L.-X. Yang, F.-T. Hsu, C.-W. Hsu, T.-W. Chang, H.-Y. Chen, L. Y.-C. Chen, Z. C. Chia, C.-H. Hung, W.-C. Su, Y.-C. Chiu, C.-C. Huang and M.-Y. Liao, Iron oxide@chlorophyll clustered nanoparticles eliminate bladder cancer by photodynamic immunotherapy-initiated ferroptosis and immunostimulation, *J. Nanobiotechnol.*, 2022, **20**, 373, DOI: 10.1186/s12951-022-01575-7.

170 X. Li, W. Xiong, Y. Wang, Y. Li, X. Cheng and W. Liu, p53 Activates the Lipoxygenase Activity of ALOX15B via Inhibiting SLC7A11 to Induce Ferroptosis in Bladder Cancer Cells, *Lab. Invest.*, 2023, **103**, 100058, DOI: 10.1016/j.labinv.2022.100058.

171 J. Hao, W. Zhang and Z. Huang, Bupivacaine modulates the apoptosis and ferroptosis in bladder cancer via phosphatidylinositol 3-kinase (PI3K)/AKT pathway, *Bioengineered*, 2022, **13**, 6794–6806, DOI: 10.1080/21655979.2022.2036909.

172 L. Shen, J. Zhang, Z. Zheng, F. Yang, S. Liu, Y. Wu, Y. Chen, T. Xu, S. Mao, Y. Yan, W. Li, W. Zhang and X. Yao, PHGDH Inhibits Ferroptosis and Promotes Malignant Progression by Upregulating SLC7A11 in Bladder Cancer, *Int. J. Biol. Sci.*, 2022, **18**, 5459–5474, DOI: 10.7150/ijbs.74546.

173 L. M. Ngema, S. A. Adeyemi, T. Marimuthu, P. Ubanako, D. Wamwangi and Y. E. Choonara, Synthesis of Novel Conjugated Linoleic Acid (CLA)-Coated Superparamagnetic Iron Oxide Nanoparticles (SPIONs) for the Delivery of Paclitaxel with Enhanced In Vitro Anti-Proliferative Activity on A549 Lung Cancer Cells, *Pharmaceutics*, 2022, **14**, 829, DOI: 10.3390/pharmaceutics14040829.

174 S. Veeramani, L. Chandrababu, I. Rajangam, N. R. Singh, L. Al-Humaid, N. D. Al-Dahmash, R. Balaji, N. Chandrasekar and M. T. Hwang, N-Hydroxysuccinamide functionalized iron oxide nanoparticles conjugated with 5-flurouracil for hyperthermic therapy of malignant liver cancer cells by DNA repair disruption, *Int. J. Biol. Macromol.*, 2023, **250**, 126001, DOI: 10.1016/j.ijbiomac.2023.126001.

175 R. Amatya, D. Kim, K. A. Min and M. C. Shin, Iron oxide nanoparticles-loaded hydrogels for effective topical photothermal treatment of skin cancer, *J. Pharm. Invest.*, 2022, **52**, 775–785, DOI: 10.1007/s40005-022-00593-9.

176 K. Skok, T. Zidarič, K. Orthaber, M. Pristovnik, N. Kostevšek, K. Ž. Žužek Rožman, S. Šturm, L. Gradišnik, U. Maver and T. Maver, Novel Methacrylate-Based Multilayer Nanofilms with Incorporated FePt-Based Nanoparticles and the Anticancer Drug 5-Fluorouracil for Skin Cancer Treatment, *Pharmaceutics*, 2022, **14**, 689, DOI: 10.3390/pharmaceutics14040689.

177 F. H. Beigi, S. S. Jazi, D. Shahbazi-Gahrouei, P. M. Khaniabadi, H. Hafezi, R. Monajemi and G. R. Amiri, Iron oxide nanoparticles coated with polydopamine as a potential nano-photothermal agent for treatment of melanoma cancer: an *in vivo* study, *Lasers Med. Sci.*, 2022, **37**, 3413–3421, DOI: 10.1007/s10103-022-03599-9.

178 E. Alphandéry, Iron oxide nanoparticles as multimodal imaging tools, *RSC Adv.*, 2019, **9**, 40577–40587, DOI: 10.1039/C9RA08612A.

179 F. Rodríguez, P. Caruana, N. De La Fuente, P. Español, M. Gámez, J. Balart, E. Llurba, R. Rovira, R. Ruiz, C. Martín-Lorente, J. L. Corchero and M. V. Céspedes, Nano-Based Approved Pharmaceuticals for Cancer Treatment: Present and Future Challenges, *Biomolecules*, 2022, **12**, 784, DOI: 10.3390/biom12060784.